HIGH ENERGY-DENSITY MATERIALS: THE ROLE OF PREDICTIVE THEORY

By

KENNETH JOHN WILSON

A DISSERTATION PRESENTED TO THE GRADUATE SCHOOL
OF THE UNIVERSITY OF FLORIDA IN PARTIAL FULFILLMENT
OF THE REQUIREMENTS FOR THE DEGREE OF
DOCTOR OF PHILOSOPHY

UNIVERSITY OF FLORIDA

2002

ACKNOWLEDGMENTS

I have relied and benefited from numerous people and many facilities during the course of my graduate studies. First, I would like to acknowledge my committee chair, Professor Rodney J. Bartlett, whose expertise and consistent enthusiasm were very much appreciated throughout my graduate career. I would also like to thank Professors N. Yngve Öhrn, Hendrik J. Monkhorst, Alexander Angerhofer, Jeffrey L. Krause, and the late Michael C. Zerner who kindly agreed to serve on my Supervisory Committee.

I am very grateful for many current and former members of the Quantum Theory Project for their interaction and support. Of special note are Dr. Ajith Perera, Professor John Watts, Professor Marcel Nooijen, Dr. So Hirata, Professor Stanisław Kucharski, Mr. Anthony Yau, Dr. Erik Deumens, Mrs. Coralu Clements and Mrs. Judy Parker. I would also like to express my gratitude to Professor Janet E. Del Bene whose research group I joined as an undergraduate student at Youngstown State University. Based on that experience, I decided to pursue a doctorate in physical chemistry at the University of Florida.

This work was supported by the United States Office of Naval Research under AASERT Award number N00014-97-1-0755, by the United States Air Force Office of Scientific Research under grant number F-49620-95-1-0130, and by the National Science Foundation under grant number 9980015. Computer facilities for many of the calculations were provided by the Department of Defense Major Shared Resource Center at the Army Research Laboratory in Aberdeen, Maryland. This dissertation was typeset with LaTeX 2_ε. I am grateful for the developers of that software, particularly Ron Smith for the creation of the ufthesis class.

TABLE OF CONTENTS

Abstract of Dissertation Presented to the Graduate School
of the University of Florida in Partial Fulfillment of the
Requirements for the Degree of Doctor of Philosophy

HIGH ENERGY-DENSITY MATERIALS:
THE ROLE OF PREDICTIVE THEORY

By

Kenneth John Wilson

May 2002

Chair: Rodney J. Bartlett
Major Department: Chemistry

This work explores several highly energetic molecular systems that might be useful as novel fuels or propellants. These systems include O_4, N_6O_3, and a series of azacubanes ($C_{8-n}N_nH_{8-n}$) along with their their nitro-substituted derivatives ($C_{8-n}N_n(NO_2)_{8-n}$). For O_4, a cooperative experimental-theoretical study was performed and a novel, long-lasting, van der Waals complex was spectroscopically observed and identified. However, another isomer of O_4, a covalently-bound D_{3h} form, seems promising as a highly energetic metastable species and merits further study. The N_6O_3 system was studied in terms of a series of nitrogen rings stablized by coordinate-covalent bonds with oxygen. Out of all of the nitrogen-ring molecules considered, N_6O_3 had the best separation of adjacent atomic charges. Consequently, it also had the most kinetic stability with a 62.4 kcal mol^{-1} activation energy toward unimolecular dissociation. The series of azacubanes were investigated as derivatives of the cubane molecule, an extremely dense, shock-insensitive explosive. The computed heats of formation for all of the azacubanes were larger than cubane's, however, none of the azacubanes have been synthesized.

To facilitate predictive calculations on other highly energetic and larger molecules, several improvements for the virtual orbital space were explored. These include virtual orbitals generated from a potential of a reduced number of electrons, virtuals generated from density functional potentials, as well as the use of approximate natural orbitals for the virtual space. Numerical results show that natural orbitals are one of the better sets and recover most of the correlation energy in a much smaller space.

CHAPTER 1
INTRODUCTION

Electronic structure theory has emerged as a powerful tool to elucidate molecular structures, energetics, and properties. Developments in the field, coupled with improvements in computer technologies, have made it fairly routine to characterize molecular systems with five or fewer atoms. Typical quantities predicted are molecular potential energy surfaces including minima and extrema, energy differences with their associated transition states and activation barriers, and normal harmonic vibrational frequencies with their infrared and Raman intensities.

The coupled-cluster (CC) framework, with an exponential ansatz, is often the method of choice for solutions to the electronic Schrödinger equation, as well as the prediction of properties [1–6]. With the demise of configuration-interaction (CI) methods in the 1990s, years of chemical literature show that CC methods are both accurate and routinely applicable. Current research efforts that add quadruple [7], pentuple [8], and higher excitations [9] (as well as the efficient construction of spin-adapted wave functions [10–12]) will allow CC theory to describe even more chemical processes.

Coupled-cluster methods have made great progress in the field of high energy-density materials (HEDMs) [13,14]. Potential HEDMs are characterized by highly energetic systems that are metastable. It is also desirable, but not required, that HEDMs be environmentally friendly. One example is liquid hydrogen and oxygen which is used as a propellant in the space shuttle [15]. Other HEDMs include monopropellants that are not combined with oxygen and that produce thrust via unimolecular dissociation to gaseous products.

Coupled-cluster methods have many strengths that make them extremely useful for the study of HEDMs. The first is their ability to survey many different types of systems. Provided that a one-particle Gaussian basis set has been developed for the elements of interest and that relativistic effects are small or included by pseudo potentials, CC methods should be applicable. In fact, a theoretical approach facilitates the construction of HEDMs by design. For instance, atoms can be easily changed within the input and substituent effects deduced. Furthermore, theoretical studies of environmentally unfriendly fuels, propellants and explosives (i.e., those that produce metals or toxic products) are safer and can be less costly than physical experiments. Also, CC methods can be highly accurate in terms of predicted bond lengths, angles and normal harmonic frequencies, and thus predictive. Often potential HEDMs exploit novel bonding patterns, or rather bonding patterns that are not yet known, so highly accurate methods are needed.

Figure 1–1. The computed CCSD(T)/aug-cc-pVTZ structure of tetrahedral N_4 (tetrazete).

One example of a molecule envisioned, characterized [16–30], and probably spectroscopically observed [31] within the HEDM effort, is the tetrahedral N_4 molecule, shown in Figure 1–1. Theoretical calculations using CC methods show that the dissociation energy for N_4 into 2 N_2 molecules is 183 kcal mol^{-1} [23] and the activation energy for this process is 61 kcal mol^{-1} [27]. Furthermore, if spin-forbidden radiationless decay is considered, the barrier is still 28.2 kcal mol^{-1} [25]. Armed with this information, several experimental groups [31, 32] attempted to prepare and spectroscopically observe N_4. Because of its high symmetry (T_d), one of difficulties is that only one vibrational mode of t_2 symmetry

is weakly active in the infrared. In fact, a weak transition was observed at 936.7 cm^{-1} which compares very well with the CCSD(T)/aug-cc-pVTZ computed value of 936 cm^{-1} [31]. However, the observed and computed frequencies for the isotopically substituted $^{15}N_4$ were somewhat less consistent with values of 900.0 cm^{-1} and 904.4 cm^{-1}, respectively. Although three vibrations (e, t_2, and a_1) are active in its Raman spectra, a higher concentration (> 80 ppm) in solid N_2 is required for detection [32].

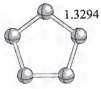

Figure 1–2. The computed CCSD(T)/aug-cc-pVTZ structure of pentagonal N_5^- (pentazole).

Another molecule of interest in the HEDM community is the pentazole ring shown in Figure 1–2. Although arylpentazoles were prepared over forty years ago [33–36], the N_5^- moiety has not yet been isolated. While it is certainly true that strong electron withdrawing groups would stabilize the five-membered nitrogen ring, a pure nitrogen anion with a large ionization potential is vitally important for the synthesis of larger nitrogen molecules. Just recently, Christe et al. reported the synthesis and characterization of the highly energetic N_5^+ molecule [37–39]. Subsequent work explored the prospects of combining N_5^+ with the azide anion (N_3^-). These attempts have not been successful and a theoretical study of the possible N_8 products showed little promise [40, 41].

With a much larger ionization potential of 5.3 eV compared to that for azide of 2.5 eV, the pentazole anion offers a more promising route toward novel nitrogen molecules. First, the pentazole anion is completely aromatic while the related neutral structure is either weakly bound or completely dissociative [42]. Second, pentazole's activation barrier for unimolecular dissociation is reasonably high (27.4 kcal mol^{-1} at the CCSD(T) level of theory [43–47]) and slightly larger than the 19.9

kcal mol^{-1} activation barrier for hydrogen pentazole [46, 48]. This suggests that pentazole would be kinetically stable if it could be prepared. Third, pentazole might exist bound to a metal atom and a recent study showed that in plane bidentate complexes are more strongly bound than metallocene-like or sandwich complexes [49]. Interesting, Gagliardi and Pyykkö [50] have proposed a larger N_7^{3-} ring with 10 π electons. Such a system, would be able to donate electrons from the δ shell to the metal.

If CC methods are to provide accurate, predictive and computationally affordable structures, energetics, and properties, a significant limitation is the dimension of the molecular orbital (MO) basis.[a] For example, the number of floating-point operations per closed-shell iteration of the coupled-cluster method with inclusion of connected single and double cluster operators (CCSD) is

$$2\frac{1}{h^2}\left(\frac{1}{4}n_{occ}^2 N_{vir}^4 + 4n_{occ}^3 N_{vir}^3\right) \tag{1–1}$$

where h is the number of symmetry operations, n_{occ} is the number of occupied orbitals, and N_{vir} is the number of virtual orbitals. Similarly, the coupled-cluster method with inclusion of connected single and double cluster operators augmented by a noniterative inclusion of triple excitations, CCSD(T), scales as

$$4\frac{1}{h^2}\left(n_{occ}^3 N_{vir}^4 + n_{occ}^4 N_{vir}^3\right) \tag{1–2}$$

Given such a power dependence (which is sometimes referred to as the exponential scaling wall [53]), it is easy to see that applications quickly become prohibitively expensive with increasing molecular size.

[a] Often, the dimension of the MO basis is the same as the primitive atomic orbital (AO) basis. The need for large AO basis sets with high angular momenta is one of the consequences of the electronic Coulomb cusp condition [51, 52].

Conversely, the power dependence as a function of the number of orbitals also displays the potential savings if a subset of the full space is used. In this dissertation, I show that frozen natural orbitals (FNOs) of a reduced dimension can be generated such that

$$N'_{vir} = xN_{vir} \qquad \text{where} \qquad x < 1 \tag{1–3}$$

Generation of FNOs in the full space is approximate (i.e., done at a lower level of theory), and hence does not involve a rate limiting step. Although FNOs are of a smaller dimension than typical canonical Hartree-Fock virtual orbitals, they still recover nearly all of the correlation energy. This translates to a savings of x^4 per iteration in the number of operations for CCSD and CCSD(T), and even larger savings for higher-level calculations. Comparisons among SCF virtual orbitals, those obtained from effective $\bar{V}_{n-1}$ and $\bar{V}_{n-\alpha}$ potentials where α is the number of valence electrons, those using density-functional theory (DFT) potentials, and FNOs will be presented.

CHAPTER 2
UNRAVELING THE MYSTERIES OF METASTABLE O_4^*[a]

Interest in tetraoxygen molecules dates to a 1924 paper by G. N. Lewis [54]; since then, studies of O_2 dimers have enjoyed a long history of investigation [55–57]. Theoretical studies of covalently bound O_4 species began with Adamantides' 1980 prediction [58] of a bound cyclic (D_{2d}) form. This stimulated considerable further theoretical effort as this cyclic O_4, nearly 4 eV higher in energy than two O_2 molecules, appeared to be a promising candidate for a high energy density material [59–61]. Subsequent theoretical studies also identified a D_{3h} form analogous to SO_3 at a somewhat higher energy [62,63]. Although experimentalists have long observed evidence of van der Waals' complexes of ground state O_2 molecules, no evidence has been found supporting the theoretical predictions of covalent O_4 species. In a recent report from the Suits' laboratory [64], 1+1 resonant photoionization spectra were reported for an energetic, metastable O_4 species produced in a DC discharge [64]. Intense spectra were observed throughout the region from 280 to 325 nm, implying an initial form of tetraoxygen containing at least 4 eV internal energy relative to $O_2 + O_2$, as well as the existence of a higher excited state through which the ionization takes place. In the absence of plausible alternatives accounting for all the observations, an energetic covalent O_4 species was considered the most likely candidate. They presented rotationally resolved

[a] This chapter consists of parts of an article reprinted with permission from Darcy S. Peterka, Musahid Ahmed, Arthur Suits, Kenneth J. Wilson, Anatoli Korkin, Marcel Nooijen, and Rodney J. Bartlett, *Journal of Chemical Physics*, volume 110, pages 6095-6098.

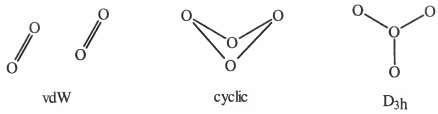

Figure 2–1. Various possible isomers of O_4.

photoionization spectra and photoelectron spectra. Here, we present the theory component that provides compelling indirect evidence pointing to the identity of this species as a novel complex, involving one ground state O_2 molecule and one in the metastable c $(^1\Sigma_u^-)$ state, but not a covalently bonded O_4.

2.1 Experimental Discussion

The experiment [64, 65] consists of passing a pulsed molecular beam of oxygen through electrodes held at ground and ± 3 to 5 kV so that the discharge occurs in the collision region of the beam. The discharge is positively biased when detecting ions, and negatively biased when detecting electrons to inhibit interference from corresponding species in the beam. The molecular beam is skimmed before entering a main chamber wherein it is crossed by an unfocused (for wavelength scans) or loosely focused (for photoelectron spectra) Nd-YAG pumped dye laser doubled to yield light tunable around 300 nm with a linewidth on the order of 0.08 cm^{-1}. The laser and molecular beams cross on the axis of a time-of-flight mass spectrometer with velocity map imaging [66] (VELMI) detector, allowing for several different kinds of experiments to be performed. Mass-selected resonant ionization scans are effected by recording the total mass-selected ion yield as a function of laser wavelength. Total photoelectron signals are similarly obtained by reversing the potentials and recording the integrated electron signal striking the detector as a function of laser wavelength. Photoelectron images are recorded on the resonant

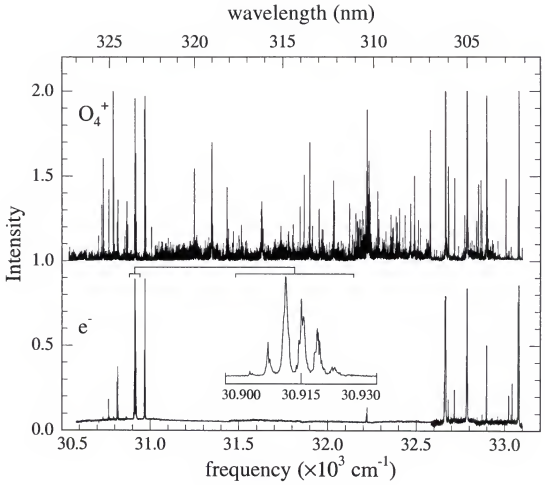

Figure 2–2. Raw O_4^+ photoion yield and total photoelectron yield spectra. Expanded region of the electron spectrum is shown in the inset.

lines using the VELMI technique, calibrated with Ar^* ionization, and converted to electron kinetic energy using established techniques.

Photoionization spectra recorded for m/e=64, O_4^+ from Suits et al. [67] are shown for the region from 302 to 325 nm in Figure 2–2. Total photoelectron yield signals are also shown; these signals are recorded under conditions in which the discharge bias is reversed and the total discharge power in the electron case is lower (2.5 Watts vs. 6 Watts). The experimentalists ascribe the differences in the ion and electron spectra to inherent noise in the higher-power ion scans and the correspondingly higher temperature of the ion scans, giving more 'hot band'

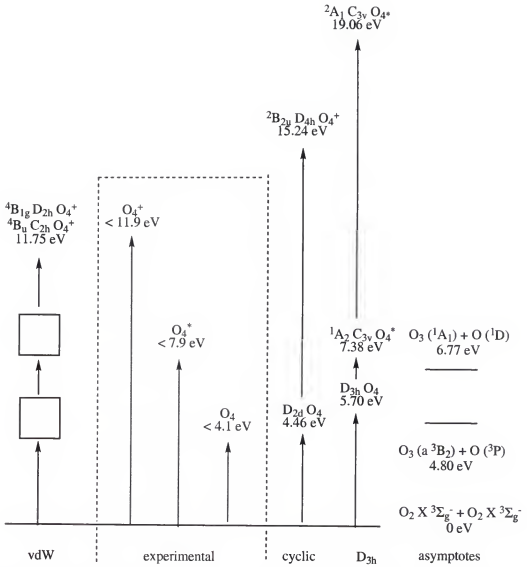

Figure 2–3. Relative energies (CCSD/TZ2P) with respect to O_2 X ($^3\Sigma_g^-$) + O_2 X ($^3\Sigma_g^-$) along different ionization paths.

contributions. Under the conditions of the experiment, virtually no ions are observed other than O_4^+. Inset in Figure 2–2 is an expanded view of the electron yield spectrum in the long wavelength region near 323 nm. Clearly resolved rotational spectra are observed, with line spacings on the order of 3.2-3.6 cm^{-1}. Similar rotational structure is also apparent on some lines in the 306 nm region, although not as pronounced.

Table 2–1. Computed CCSD and CCSD(T) relative energies and rotational constants at optimal geometries for O_4 species. The relative energies, in units of electron Volts, are with respect to O_2 X ($^3\Sigma_g^-$) + O_2 X ($^3\Sigma_g^-$) and rotational constants are from CCSD(T) geometries in cm^{-1}. Also shown are the lowest vertical ionization potentials for the two covalently bound forms of O_4. The nuclear geometry for these calculations was the optimized CCSD(T)/TZ2P for the ground state.

		CCSD	CCSD(T)	rotational constants (B_e)			IP
	$^1A_1$ D_{2d}	4.56	4.16	0.254	0.478	0.478	10.98
	$^2B_{2u}$ D_{4h} ionized state	15.28	14.68	0.260	0.520	0.520	
covalent	$^1A_1'$ D_{3h}	5.80	5.07	0.204	0.408	0.408	12.47
	$^1A_2$ C_{3v} excited state[a]	7.37		0.208	0.406	0.406	
	$^4A_2$ C_{3v} ionized state	17.43	17.40	0.194	0.368	0.368	
vdW	^4B_u C_{2h} ionized state	11.83	11.57	0.149	0.185	0.769	
	$^4B_{1g}$ D_{2h} ionized state	11.83	11.57	0.149	0.185	0.769	

a.) For this species, rotational constants are from the EE-EOM-CCSD geometry.

2.2 Theoretical Discussion

If one of the covalent species is responsible for these spectra, then two critical issues are 1) accounting for the observed ionization potential of ~8 eV from the metastable state or likely 12 eV or so from two ground state O_2 molecules, and 2) finding a bound excited state ~4 eV above the metastable species. To this end, we have performed accurate coupled-cluster (CC) calculations with the ACES II program system [68]. We use a TZ2P basis [69] of Cartesian Gaussians contracted as (11s6p3d)/[5s3p2d] except as indicated. Table 2–1 presents computed CCSD and CCSD(T) [1,2] energies relative to two ground state O_2 molecules for several states of interest. At the CCSD(T) level, we find two covalent forms: the cyclic (D_{2d}) at 4.16 eV and the pinwheel (D_{3h}) at 5.07 eV. We also obtained detailed structures and vibrational frequencies (shown in Table 2–2) for these two species and IP-EOM-CCSD [1,2] vertical ionization potentials for the two covalent forms. The lowest IPs occur at 10.98 for the cyclic and 12.47 for the pinwheel structures. However, this is much higher than the energy of two photons at 300 nm (~8 eV), thus outside the range of the experiment. Also shown in Table 2–1 are the energies of the ionized van der Waals complexes: our result of 11.57 eV is in excellent agreement with the 11.67 eV CASSCF value of Lindh and Barnes [70]. Also shown in Table 2–1 are rotational constants for these species. These are not consistent with the rotationally resolved spectra in the inset in Figure 2–2. Even accounting for the nuclear spin symmetry for the D_{3h} species, a line spacing on the order of $6B_e$ or 1.2 cm^{-1} is the largest expected.

The other question pertains to the existence of a bound excited state of the covalent species that is 4 eV above the metastable species and whose vibrational frequencies were previously estimated [64]. A STEOM-CC [71] calculation in the POL1 basis at the geometry of the D_{2d} ground state shows a weakly allowed E state at 7.10 eV and a dipole forbidden A_2 state at 8.54 eV and three others weakly

Table 2–2. Optimized structures in ångstroms and degrees, normal harmonic vibrational frequencies in cm^{-1} and their associated intensities in parenthesis with units of km mol^{-1} of various O_4 isomers computed within the TZ2P basis.

		HF	MBPT(2)	MBPT(4)	CCSD	CCSD(T)
	R	1.392	1.483	1.498	1.460	1.486
	dihedral	20.4	28.8	28.9	26.6	27.9
	a_1	353	411	401	402	400
$^1A_1$ D_{2d}	e	1107	703	652	816	702(0.0)
	b_2	1062	779	758	856	798(0.1)
	b_1	1245	851	797	930	809
	a_1	1222	895	844	985	897
	R	1.876	2.056	2.040	1.975	2.012
	b_{2u}	405			329	292
$^2B_{2u}$ D_{4h} cation	b_{1g}	1250			975	898
	a_{1g}	1359			1064	961
	b_{2g}	1468			1184	1086
	e_u	999i			1342	852(0.1)
	R	1.240	1.304	1.326	1.290	1.312
	e'	596	631	584	585	559(5.4)
$^1A_1'$ D_{3h}	a_2''	779	666	608	666	609(1.7)
	e'	1026	1861	1476	1030	988(186.2)
	a_1'	1035	928	817	902	828
	R		1.324		1.330	
	angle		157.7		155.7	
$^1A_2$ C_{3v} excited state	e		188		126(4.6)	
	a_1		492		485(4.6)	
	e		1252		717(9.6)	
	a_1		936		867(0.3)	

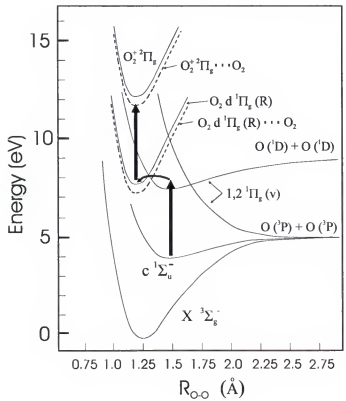

Figure 2–4. Relevant potential curves adapted from Reference [73], from calculations of Reference [74]. The Rydberg and ion curves, duplicated and offset -0.45 eV (the energy of the O_2–O_2^+ bond) are shown as dashed lines.

allowed, between 9.2 and 10.0 eV. For the D_{3h} form, the first state is a forbidden A_1'' that occurs at 7.24 eV with a strong E' state at 8.92 eV, with the next E' state at 12.93 eV. There are five triplet states in the range of 6 to 9 eV for the D_{2d} form, with the lowest at 6.26. The triplet states start at 7.07 eV for the D_{3h} isomer, with an E' state at 7.60. However, despite extensive effort, when optimizing the geometry for excited states either with CCSD when applicable, or EOM-CCSD analytical gradient techniques [72] to determine if there were bound excited states, only one singlet state was found. Neither the energy (shown in Table 2–1) nor the frequencies (shown in Table 2–2) make a persuasive case for this being the possible intermediate state in the 1+1 experiment. Taking all these points into consideration, covalently bound energetic tetraoxygen molecules do not appear likely to be responsible for the experimental observations.

We now consider electronically excited van der Waals complexes. There are several metastable states of O_2 that may form long-lived van der Waals complexes of the correct energy. The relevant potential energy curves for O_2 are shown in Figure 2–4. Complexes involving lower lying metastable singlet states are known, but have neither sufficient energy nor plausible ionization paths to be responsible for the experimental observations. The Herzberg states of O_2, however, do appear at the correct energy to form complexes that could give rise to the observed spectra. One of these, the c $(^1\Sigma_u^-)$ state, is shown in Figure 2–4 based on calculations of Saxon and Liu [74], adapted from van der Zande et al [73, 75]. This is the only species that may possess an allowed optical transition in this wavelength region: an excited 1 $(^1\Pi_g)$ state exists very near the energy of our probe transition (i.e., about 4 eV above this c state). However, earlier calculations indicated that this 1 $(^1\Pi_g)$ state is repulsive, adiabatically correlating with two ground state oxygen atoms. In an illuminating series of experiments [73, 75] studying atomic fragments after charge transfer from cesium atoms to O_2^+, van der Zande et al. explored the nonadiabatic dynamics and coupling among several of the curves in Figure 2–4 (and with triplet curves not shown). Most importantly, they showed that the 1 $(^1\Pi_g)$ and 2 $(^1\Pi_g)$ curves shown in Figure 2–4 do not interact strongly, and may be viewed in a 'diabatic' picture, as shown; the 1 $(^1\Pi_g)$ level is a bound or quasibound state. The 1 $(^1\Pi_g) \leftarrow$ c $(^1\Sigma_u^-)$ transition of O_2 is thus a strongly allowed optical transition in O_2 with nearly diagonal Franck-Condon factors in the region of 280-330 nm. It is not clear that this important implication of the observations of van der Zande et al. had been recognized.

However, direct ionization of this 1 $(^1\Pi_g)$ state is not possible in this wavelength region, since the Franck-Condon factors connecting it with the ground state of the ion are negligible. In fact, the experiments of van der Zande and coworkers show the importance of the interactions involving the 1 $(^1\Pi_g)$ valence state and the d $(^1\Pi_g)$

Rydberg state that was initially prepared in their experiments. This shows a path to ionization in this wavelength region via the valence-Rydberg interactions. These considerations yield the following scenario for this 1+1 ionization process in O_4^*, indicated by the heavy arrows in Figure 2–4. If we begin with a van der Waals complex between O_2 X $(^3\Sigma_u^-)$ and O_2 c $(^1\Sigma_u^-)$, a fully allowed electronic transition localized on the c state molecule takes us to a complex involving the 1 $(^1\Pi_g)$ state.

This state can either predissociate to give oxygen atoms (and an O_2 molecule), or couple to the d $(^1\Pi_g)$ Rydberg state; or the system can dissociate to two O_2 molecules. It is likely that all of these occur, no doubt with a strong dependence on the initially excited vibrational level. If the Rydberg complex is formed, it can then ionize easily in this wavelength region, and the ionization will be dominated by $\Delta v = 0$ transitions owing to the diagonal Franck-Condon factors between the Rydberg and the ion. If this picture is accurate for O_4, it is surprising that no O_2^+ is seen; this implies some significant differences for the ionization dynamics in the complex as opposed to the free O_2 molecule. In fact, it is precisely in the nature of these Rydberg-valence interactions that we can expect a profound impact of the formation of the van der Waals complex. This is because the Rydberg state will be greatly stabilized in the complex—nearly to the extent of the 0.45 eV bond in O_2–O_2^+. The valence state curves will be little-perturbed in comparison. The location of the Rydberg and ion curves for the complex are shown as dashed lines in Figure 2–4. This provides a reasonable explanation for the absence of the O_2^+ in these experiments despite the likelihood that the number density of free O_2 c $(^1\Sigma_u^-)$ molecules is much greater than those involved in complexes. The fate of the free O_2, upon excitation to the 1 $(^1\Pi_g)$ state, is either predissociation via the 2 $(^1\Pi_g)$ state, or by the triplet states interacting with the d state.

Many of the experimental results can be satisfactorily accounted for by invoking this complex. The rotational spacing in the long wavelength region, about

3.5 cm^{-1}, is very near $4B_e$ for the c $(^1\Sigma_u^-)$ state ($B_e = 0.9$ cm^{-1}). This would be expected, for example, for a T-shaped complex wherein one of the rotational constants will resemble that of one of the O_2 molecules. The photoelectron spectra, dominated by single peaks, arise because the ionization takes place from a complex involving the d $(^1\Pi_g)$ Rydberg state so that $\Delta v = 0$ transitions dominate as mentioned above. Finally, the absence of O_2^+ is readily explained by the very different Rydberg-valence interactions in the complex as opposed to the free O_2. This picture also accounts for some unusual spectra reported in a closely related study by Helm and Walter [76]. Their experiments were similar to the studies of van der Zande et al., but used charge transfer to O_4^+ rather than O_2^+. They reported clearly resolved vibrational structure in the O_2 product kinetic energy distributions after charge transfer from cesium, which they reluctantly ascribed to coincident formation of two O_2 molecules in v=29, a rather unlikely process. This was necessary to account for the vibrational spacing of 800 cm^{-1} observed in the O_2 kinetic energy release distributions. Our alternative interpretation of their results suggests simply the reverse of the ionization process outlined above: electron transfer from cesium populates the Rydberg state around 7.6 eV, which then couples efficiently to the metastable O_2 X $(^3\Sigma_g^-)$—O_2 1 $(^1\Pi_g)$ complex. We suggest that the structure in the kinetic energy release distributions of Helm and Walter simply reflects the vibrational structure in the metastable state. For the Herzberg states, the vibrational frequencies are all on the order of 800 cm^{-1}; the vibrational frequency in the 1 $(^1\Pi_g)$ state is likely to be similar.

It is important to note that although these spectra are not associated with covalently bound, energetic O_4 species, they may well be present in the molecular beam.

CHAPTER 3
STABILIZATION OF THE PSEUDO-BENZENE N_6 RING WITH OXYGEN[a]

3.1 Introduction

One of the goals for the development of new high-energy-density molecules has been to explore the prospects for making novel polynitrogen compounds. Since the generation of N_2 as a propulsion or explosion product is highly recommended by its very strong triple bond,

citehedmabstract,lauderdale,ferris,korkin,nreview,polynitrogen,perera have used predictive quantum chemical techniques to investigate the structure, stability, spectra, and decomposition paths of experimentally unknown polynitrogen molecules, as have others [15, 25, 77–79]. (See Reference [80] for an extensive survey of pure nitrogen species, from 2 to 12 atoms, their cations, anions and low-lying excited states). It is apparent that if -CH groups could be replaced by isovalent -N, there will be a large increase in the amount of energy stored by virtue of the standard state of nitrogen, N_2, and also in the repulsion of electron lone pairs on adjacent nitrogens. However, we pay a price for this endothermicity, since to retain the energy for use as a fuel, we must have sufficiently high activation barriers to unimolecular decomposition as well, and we have also to address the question of whether non-radiative transitions can play a role in the molecule's decomposition [25]. We have considered the molecule N_4 in a tetrahedral arrangement [21, 24, 28], as well as the N_8 analog of cubane [24, 81]. In both cases,

[a] This chapter consists of an article reproduced with permission from Kenneth J. Wilson, S. Ajith Perera, Rodney J. Bartlett, and John D. Watts, *Journal of Physical Chemistry A* volume 105, 7693-7699.

the high symmetry indicates that any decomposition to N_2 would be Woodward-Hoffman forbidden, suggesting significant barriers to decomposition. Numerical investigation of the barriers shows that N_4's is 62 kcal mol^{-1} [27,77] though its effective barrier is close to 30 (because of a low-lying triplet state [25,27]) and N_8's is 19 [15,79]. In Chapter 4 of this dissertation, we have also investigated the other azacubanes where 1-7 of the -CH units have been replaced by -N, and the nitroazacubanes. More energy per molecule can be gained from single rather than double-bonded nitrogen linkages, recommending N_4 and N_8 if they could be synthesized and stabilized, but at the cost of the stability offered by the double-bonded -N=N- structures. In addition, to impose some organization of proposed energetic species, we here consider dimers, trimers, etc. of highly energetic units such as O_2NCN and other units [82]. In this paper, the unit is N_2O.

Beyond N_2 and N_3^-, there is little experimental evidence to date that nitrogen can form stable homonuclear molecules. Just recently, Christe and coworkers have reported the synthesis of $N_5^+AsF_6^-$ [37] while N_3^+ [83], N_4^+ [84–86] and the diazidyl N_6^- complex [87,88] have been detected spectroscopically as short-lived species. Notable in the series of homoleptic polynitrogen systems is the absence of the N_6 ring. The N_6 ring, analogous to benzene, is not a minimum on the potential energy surface as a planar, hexagonal ring. Instead, including electron correlation, the D_{6h} structure is a second-order saddle point with the closest minimum, a non-planar boat-type D_2 structure [89]. This feature might be attributed to the large lone-pair repulsion in the ring. However, we might expect to reduce some of this repulsion by forming coordinate covalent bonds, -N→O. In fact, such bonds are found in explosives [90–93] and suggest some interesting consequences for the formation of novel polynitrogen rings.

Table 3–1. Computed electronic energies in Hartrees with the 6-31G* basis for the nitrogen ring systems considered in this work along with their transition states for unimolecular dissociation and the reference systems (N_2, O_2 and N_2O).

	Symmetry	SCF	MBPT(2)	CCSD	CCSD(T)	B3LYP
N_4O	C_{3v}	-292.24948	-293.14183	-293.11678	-293.16431	-293.74738
N_4O TS	C_s		-293.12807	-293.10008	-293.15494	-293.73555
N_4O_2	C_{2h}	-367.18793	-368.22286	-368.21021	-368.26495	-369.00953
N_4O_2 TS	C_s	-367.08451	-368.11780	-368.13412		-368.94015
N_6O	C_s	-401.23971	-402.41983	-402.40314	-402.46850	-403.27751
N_6O TS	C_1	-401.20786	-402.41173	-402.39816	-402.46492	-403.27193
N_6O_2	C_{2v}	-476.03554	-477.40901	-477.38679	-477.46083	-478.42721
N_6O_2 TS	C_1	-476.00358	-477.37440	-477.36196	-477.43747	-478.40574
N_6O_3	D_{3h}	-550.82526	-552.39317	-552.36192	-552.44360	-553.56742
N_6O_3 TS	C_1	-550.65752	-552.28431	-552.23772	-552.33575	-553.44754
N_2	$D_{\infty h}$	-108.94395	-109.25528	-109.25579	-109.26852	-109.47195
O_2	$D_{\infty h}$	-149.61791	-149.94973	-149.95176	-149.96178	-150.26010
N_2O	$C_{\infty v}$	-183.68012	-184.20414	-184.18702	-184.21223	-184.57778

3.2 Computational Methods

All the *ab initio* calculations in this report were performed with the ACES II program system [68] while the density functional calculations were performed with the Q-CHEM computer program [94]. The well-known hierarchy of *ab initio* methods ranging from: Hartree-Fock self-consistent field (SCF), second-order many-body perturbation theory (MBPT(2)), coupled-cluster singles and doubles (CCSD) to coupled-cluster singles and doubles with a perturbative inclusion of triples (CCSD(T)) were employed to show the importance of higher dynamic correlation. Density functional theory with the empirical Becke three-parameter Lee, Yang and Parr (B3LYP) exchange correlation functional was also used. Both the *ab initio* and DFT calculations were performed in the 6-31G* one-particle basis set using Cartesian Gaussians [69]. This basis corresponds to a modest 15 functions per heavy atom, but is largely sufficient for the whole series of molecules ranging up to nine heavy atoms, studied here. To obtain better energetics, single point energies were computed with the aug-cc-pVDZ basis set [95] at the optimized 6-31G* geometries (see Table 3–1). Total atomic charges were computed with the natural bond orbital (NBO) procedure of Weinhold et al [96]. A spin unrestricted wave function was used to describe the X $({}^3\Sigma_g^-)$ state of O_2 which showed little evidence of spin contamination. All transition states were confirmed by the presence of only one negative eigenvalue in the computed Hessian matrix. All core electrons were omitted from the correlation procedure, however, the virtual orbitals corresponding to the core electrons where included in the correlated calculation.

3.3 Results and Discussion

In this section, we begin by checking the reliability of our methods by calculations on the N_2O molecule. Then, we explore the trends in structures and energetics for its dimers and trimers plus related species as a function of increasing the number of coordinate–covalent bonds. The first series is based on a

1.092	1.178 SCF
1.172	1.193 MBPT(2)
1.136	1.201 CCSD
1.148	1.205 CCSD(T)
1.134	1.193 B3LYP
1.127	1.185 exp

Figure 3–1. Computed and experimental structure for N_2O.

four-membered nitrogen-ring system and contains: N_4O and N_4O_2. In the second series, we consider the six-membered nitrogen-ring systems: N_6O, N_6O_2 and N_6O_3.

The computed and experimental geometries of N_2O are shown in Figure 3–1. The SCF method slightly underestimates both bond lengths, while all other methods predict bond lengths longer than their experimental values. The computed CCSD(T) N-N bond length of 1.148 Å and N-O bond distance of 1.205 Å compare to the experimental values of 1.127 Å and 1.185 Å, respectively. The error is due in large part to the use of the small 6-31G* one-particle basis set, as the larger cc-pVTZ basis gives 1.132 Å and 1.189 Å. However the predicted B3LYP bond lengths seem slightly better in the 6-31G* small basis. The computed and experimental harmonic frequencies are presented in Table 3–2. Here, the CCSD(T) computed frequencies are slightly better than the B3LYP computed values. The largest difference is for the second Σ_g^+ normal mode which CCSD(T) underestimates by 6 cm^{-1} and the B3LYP method overestimates by 88 cm^{-1}.

The first member of the N_4 series is the N_4O system and its computed lowest-energy structure is shown in Figure 3–2. The four-membered nitrogen ring is not a minimum for this molecule which instead adopts a C_{3v} structure similar to that of the tetrahedral isomer of N_4. One of the N-N bond lengths is on the order of a single bond (1.45 Å [99]) with its CCSD(T) predicted value of 1.458 Å and the other one that is not equivalent by symmetry has a slightly longer value of 1.536 Å. Other isomers of N_4O have been considered including a C_{2v} ring structure with oxygen as part of the ring [100]. However, the transition state for the unimolecular

Table 3–2. Computed harmonic vibrational frequencies in cm^{-1} and infrared intensities in parentheses with units of km mol^{-1} for the N_2, O_2 and N_2O molecules. All computed values are from the 6-31G* basis.

	Symmetry	SCF	MBPT(2)	CCSD	CCSD(T)	B3LYP	experiment [97,98]
$^1\Sigma_g^+$ N_2 ($D_{\infty h}$)	Σ_g^+	2758	2175	2411	2341	2457	2358.57
$^3\Sigma_g^-$ O_2 ($D_{\infty h}$)	Σ_g^+	1998	1410	1650	1578	1658	1580.19
	Π	689	575	597	573(6.8)	603(9.0)	596.3
$^1\Sigma^+$ N_2O ($C_{\infty v}$)	Σ^+	1393	1288	1319	1292(42.4)	1342(49.9)	1298.3
	Σ^+	2633	2247	2353	2276(287.5)	2370(308.9)	2282.1

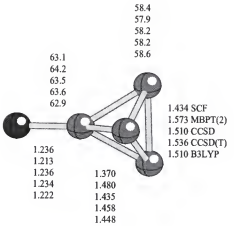

Figure 3–2. Computed structure for N_4O.

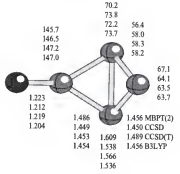

Figure 3–3. Computed transition state structure for N_4O.

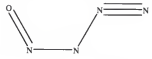

Figure 3–4. Lewis structure of *trans*-nitrosyl azide.

dissociation of this C_{2v} molecule was located which indicated a barrier between 1 and 2 kcal mol^{-1}. A somewhat more stable and experimentally-observed [101] isomer is the *trans*-nitrosyl azide shown in Figure 3–4. Prompted by its Raman characterization, Klapötke and Schulz considered two dissociation pathways for this molecule [102]. The first pathway involved conversion into a cis isomer, then a cyclic form, followed by its dissociation into N_2 and linear N_2O. The highest barrier for this process computed at the MP2/6-31+G* level was 6.7 kcal mol^{-1}. A transition

Table 3–3. Activation energies in kcal mol^{-1} for unimolecular dissociation. Values not in parentheses are from the aug-cc-pVDZ basis at the 6-31G* optimized geometries. All values include electronic energy differences as well as zero-point vibrational energy differences and thermodynamic corrections for 298 K.

	SCF	MBPT(2)	CCSD	CCSD(T)	B3LYP
N_4O		8.6 (9.3)	9.3 (10.0)	5.0 (5.6)	6.4 (-1.0)
N_4O_2	60.1 (60.1)	65.0 (65.4)	44.8 (45.6)		41.1 (41.4)
N_6O	17.9 (18.5)	3.4 (4.0)	1.8 (1.8)	1.1 (1.2)	2.3 (2.8)
N_6O_2	18.4 (19.2)	20.4 (21.3)	13.9 (14.5)	13.1 (13.8)	12.0 (12.6)
N_6O_3	101.2 (86.3)	64.9 (66.6)	74.1	62.4	71.9 (74.7)

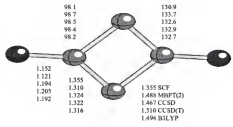

Figure 3–5. Computed structure for N_4O_2.

state for the direct dissociation into N_2 and cyclic N_2O was also found which indicated a barrier of 24.2 kcal mol^{-1}.

The transition state structure for the loss of NO from our C_{3v} structure is shown in Figure 3–3. It has C_s symmetry with the major difference that one of the N-N bonds is broken. It is worth noting that the differences between the MBPT(2), CCSD, CCSD(T) and B3LYP methods are slightly larger than those for the structure shown in Figure 3–2, indicating that more sophisticated treatments of electron correlation are needed to describe transition states. The barriers, shown in Table 3–3, differ at most by 7 kcal mol^{-1} from our most reliable estimate, the CCSD(T) value of 5.6 kcal mol^{-1}. Such a small value suggests that it may be possible to observe this N_4O isomer only as a short-lived species, rather than being suitable for preparation and handling in bulk quantities.

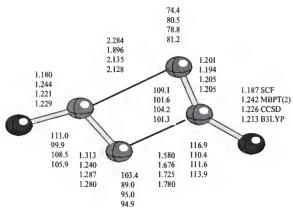

Figure 3–6. Computed transition state structure for N_4O_2.

The addition of a second oxygen atom to the N_4 ring leads to the completely planar N_4O_2 structure shown in Figure 3–5. The optimized SCF structure belongs to the D_{2h} point group while all other methods predict a less symmetric C_{2h} structure. One N-N bond length is between that of a single (1.45 Å) and double (1.25 Å) bond and the other, not equivalent by symmetry, is slightly longer than a typical single bond. Previously, Manaa and Chabalowski have considered another cyclic isomer of N_4O_2 where the oxygen atoms were members of the ring [103]. This structure does not allow for oxygen to remove as much charge from the nitrogen atoms and hence is not as stable kinetically.[b] For the linear N_4O_2 isomer, there have been two reports of its synthesis [104, 105].

The addition of the second coordinate covalent bond to the four-membered ring significantly increases its kinetic stability. The transition state structure for the loss of N_2O is presented in Figure 3–6. This structure has C_s symmetry and two considerably longer N-N bonds. The large differences between the SCF and CCSD

[b] The barrier for the unimolecular dissociation of the N_4O_2 boat isomer is 11.0 kcal mol^{-1} at the CCSD(T)/6-31G* level. Watts, J. D.; Wilson, K. J.; Bartlett, R. J. unpublished work.

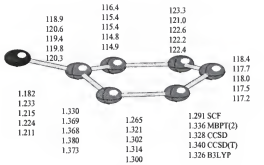

Figure 3–7. Computed structure for N_6O.

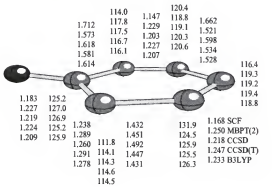

Figure 3–8. Computed transition state structure for N_6O.

structures demonstrate the importance of electron correlation in describing the transition state. Furthermore, there is a 14 kcal mol^{-1} difference in activation energies with the SCF computed value of 60.1 kcal mol^{-1} and the CCSD value of 45.6 kcal mol^{-1}. Because of large T_2 amplitudes, we were unable to converge the CCSD(T) method on this transition state.

The N_6O molecule is the first member of the second series with a six-membered ring. Its structure is nonplanar with C_s symmetry as shown in Figure 3–7. All N-N bond lengths are greater than that of a double bond (1.25 Å), but shorter than a single bond (1.45 Å [99]). One interesting aspect of the frequencies and intensities in Table 3–6 is the substantial difference in the B3LYP and CCSD(T) intensities. Particularly, the three a' modes near 1000 cm^{-1} have a different distribution of intensities, though the total intensity in that symmetry is comparable.

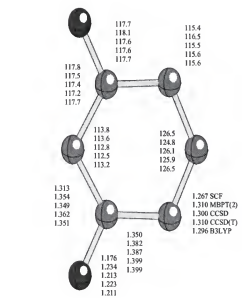

Figure 3–9. Computed structure for N_6O_2.

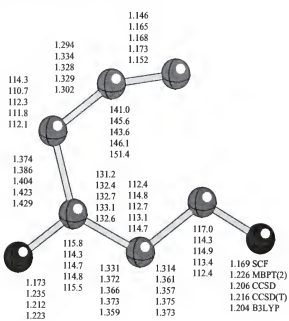

Figure 3–10. Computed transition state structure for N_6O_2.

The transition state for the unimolecular dissociation of N_6O is shown in Figure 3–8 which corresponds to loss of N_2. Our best estimate of the barrier for this process is 1.2 kcal mol^{-1} at the CCSD(T)/aug-cc-pVDZ//CCSD(T)/6-31G* level of theory.

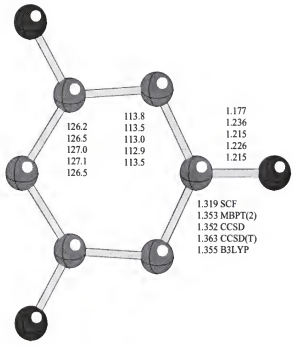

Figure 3–11. Computed structure for N_6O_3.

Addition of another oxygen atom to the previous structure results in the planar N_6O_2 system shown in Figure 3–9. This molecule has C_{2v} symmetry and all N-N bond lengths are between those of a double and single bond. Again, the IR intensities, shown in Table 3–6 vary greatly between CCSD(T) and B3LYP.

The transition state for unimolecular dissociation is shown in Figure 3–10 and corresponds to loss of N_3. The barrier for this process is 13.8 kcal mol^{-1} at the CCSD(T)/aug-cc-pVDZ//CCSD(T)/6-31G* level. Although this value is somewhat larger than that for N_6O, it is still too low to facilitate handling on a bulk scale. Other transitions might occur to products involving N_3^- and N_3O^+, the latter isovalent to N_4.

Addition of another oxygen results in the highly symmetric N_6O_3 structure shown in Figure 3–11, the trimer of N_2O. This molecule has D_{3h} symmetry with all N-N bond lengths equal to 1.363 Å at the CCSD(T) level of theory. This distance is almost exactly between that of a double and single bond, attesting to benzene-like

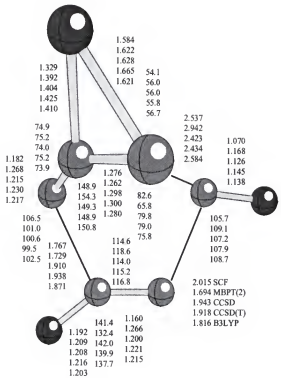

Figure 3–12. Computed transition state structure for N_6O_3.

delocalization (though no resonance stabilization as discussed in Section 3.5). Unlike N_6O and N_6O_2, N_6O_3 has comparable IR intensity patterns between B3LYP and CCSD(T).

The transition state for unimolecular dissociation is shown in Figure 3–12. Our best estimate at the CCSD(T)/6-31G* level for the barrier of this process is 62.4 kcal mol^{-1}. Being the trimer of N_2O, there could be an alternative dissociation path to 3 N_2O's, analogous to the concerted triple dissociation of s-tetrazine [106], however all attempts to locate other transition states along different dissociation pathways were unsuccessful. Initial indications are that such a N_6O_3 species should be capable of being synthesized.

3.4 Atomic Charges

One property which can be related to the computed activation energies is the computed atomic charges or rather the arrangement of the atomic charges. These

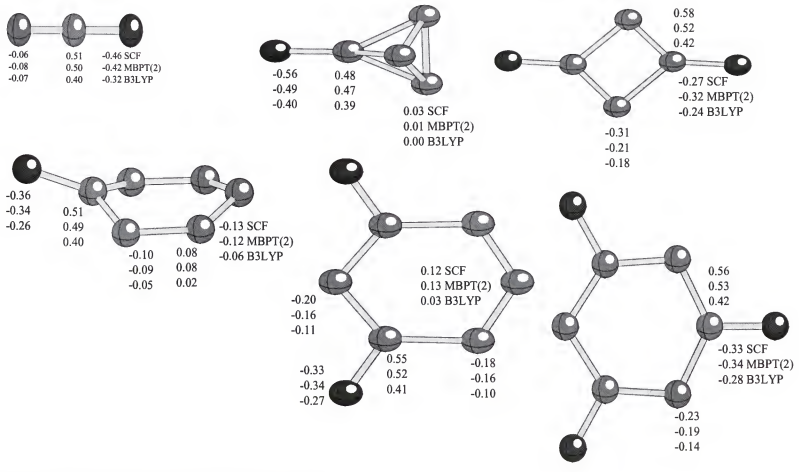

Figure 3–13. Computed NBO natural atomic charges.

were computed with the natural bond orbital (NBO) formalism [107] within the 6-31G* basis and are presented in Figure 3–13. In all structures, oxygen has a large negative charge. However, in the stable structures (N_4O_2 and N_6O_3), the nitrogen ring is composed of alternating charges. For example in N_4O_2, the smallest charge difference on adjacent nitrogens is 0.60 at the B3LYP level of theory. In N_6O and N_6O_2, the charge on adjacent nitrogens is not as well separated with the smallest B3LYP differences being 0.07 and 0.13, respectively. Figure 3–13 shows a perfectly alternating NBO charge on the six-membered ring of N_6O_3 with the smallest charge difference being 0.56.

3.5 Resonance Stabilization?

Another interesting concept with the proposed highly energetic molecules is their resonance energy and whether they are resonance stabilized. Early calculations on planar-hexagonal N_6 based on Shaik's quantum-mechanical resonance energy [108] and Dewar's π-resonance energy [109] indicated that hexazine was even more aromatic than benzene. However, Glukhovtsev and Schleyer later reported homodesmic and hyperhomodesmic reactions for hexazine which showed a destabilizing resonance energy of 17.6 kcal mol^{-1} and 10.4 kcal mol^{-1}, respectively [110, 111].

Gimarc and Zhao have offered an explanation of nitrogen's destabilizing resonance energy as opposed to that of carbon's, which is based on average bond energies [112, 113]. In this approximation, the total energy of a molecule is the sum of its bond energies. Since the average carbon-carbon single bond energy is 83 kcal mol^{-1} which is more than half of the carbon-carbon double bond energy of 144 kcal mol^{-1}, carbon structures with pairs of single bonds rather than double bonds are lower in energy. For nitrogen, the situation is reversed. The average nitrogen-nitrogen single bond energy is 43 kcal mol^{-1}, which is less than half of the

nitrogen-nitrogen double bond energy of 100 kcal mol^{-1}. Hence, nitrogen prefers double bonds rather than pairs of single bonds.

To estimate the amount of resonance energy in the novel N_4O_2 and N_6O_3 molecules, we have used the following isodesmic reactions, in analogy to $N_6 + 3\ NH_3 \longrightarrow 3\ H_2N\text{-}N{=}NH$.

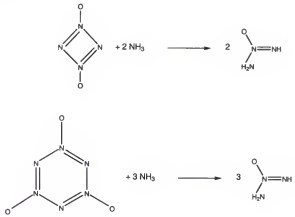

Figure 3–14. Isodesmic reactions for N_4O_2 and N_6O_3.

Based on the energies of the isodesmic reactions shown in Figure 3–14, both ring structures have a destabilizing resonance energy. For N_4O_2, the CCSD(T)/aug-cc-pVDZ//CCSD(T)/6-31G* value is 27.6 kcal mol^{-1} and for N_6O_3, 13.9 kcal mol^{-1}. Other quantum mechanical methods predict values which agree closely with CCSD(T) and they are presented in Table 3–4. We also present the resonance energy for N_6 in the D_{6h} conformation. In fact, the value of -17.6 is very close to our MBPT(2)/6-31G* value for N_6O_3 of -18.6 kcal mol^{-1}. For N_4O_2, the resonance energy is slightly more destabilizing, numerically being -36.4 kcal mol^{-1}.

3.6 Enthalpy of Formation and Specific Impulse

One useful figure of merit for potential fuels and explosives is the material's enthalpy of formation, ΔH_f, or energy relative to the elements in their standard states. It has been shown for molecules that do not contain fluorine, the enthalpy of formation largely parallels the heat of combustion [115]. In Table 3–5, we present ΔH_f's for the ring molecules considered in this work and the N_2O test system. For

Table 3–4. Resonance energies in kcal mol^{-1} for isodesmic reactions. Values not in parentheses are from the 6-31G* basis, and values in parentheses are from the aug-cc-pVDZ basis at the 6-31G* optimized geometries. All values include electronic energy differences as well as zero-point vibrational energy differences and thermodynamic corrections for 298 K.

	SCF	MBPT(2)	CCSD	CCSD(T)	B3LYP
N_4O_2	-38.5 (-34.4)	-36.4 (-32.1)	-36.5 (-31.6)	-32.3 (-27.6)	-35.2 (-32.5)
N_6O_3	-32.1 (-26.2)	-18.6 (-10.7)	-26.5 (-18.1)	-22.0 (-13.9)	-20.3 (-15.9)
$N_6(D_{6h})$		-17.6[a]			
$(CH)_6$		23.9[a]			

a.) These values were computed with the MBPT(4)/6-31G*//MBPT(2)/6-31G* formalism [110, 111].

Table 3–5. Enthalpy of formation (ΔH_f) and specific impulse (I_{sp}) values for the ring species considered in this work. ΔH_f is in units of kcal mol^{-1} and I_{sp} is in seconds. Values not in parentheses are from the aug-cc-pVDZ basis at the 6-31G* optimized geometries. All values include electronic energy differences as well as zero-point vibrational energy differences and thermodynamic corrections for 298 K.

	ΔH_f		I_{sp}	
	B3LYP	experiment [114]	B3LYP	experiment[a]
N_2O	16.7 (17.3)	19.61	163.2 (166.3)	176.9
N_4O	205.2 (206.4)		447.3 (448.6)	
N_4O_2	125.4 (125.0)		316.3 (315.8)	
N_6O	169.1 (169.3)		344.5 (344.7)	
N_6O_2	160.4 (160.2)		311.5 (311.4)	
N_6O_3	155.6 (154.7)		287.7 (286.8)	

a.) Calculated using the experimental ΔH_f and Equation 3–1.

N_2O, the ΔH_f computed from B3LYP/aug-cc-pVDZ//B3LYP/6-31G* is 17.3 kcal mol^{-1} which is in excellent agreement with the experimental value of 19.61 kcal mol^{-1} [114]. For propellants, the molecular weight is also important and a material's potential is best measured by its specific impulse, I_{sp}. The specific impulse in units of seconds can be approximated with the equation [116]:

$$I_{sp}(\text{seconds}) = 265\sqrt{\frac{\Delta H_f(\text{kcal mol}^{-1})}{MW(\text{grams mol}^{-1})}} \tag{3–1}$$

where MW is the molecular weight in grams per mol. The I_{sp}'s for the ring species considered in this work are presented in Table 3–5. The prospective HEDMs that are stable with respect to unimolecular dissociation, N_4O_2 and N_6O_3, have I_{sp}'s of 315.8 and 286.8 seconds, respectively. Both of these offer an improvement to the 224 seconds I_{sp} for hydrazine, the most frequently used monopropellant. A survey of possible generalizations of the basic hydrazine molecular structure has been considered elsewhere [117].

Table 3–6. Computed normal harmonic vibrational frequencies and infrared intensities in parentheses for various nitrogen ring structures within the 6-31G* basis except for the CCSD(T) frequencies of the N_6O_3 isomer which were computed with the larger cc-pVDZ basis set. Frequencies are in units of cm^{-1}, intensities are in km mol^{-1}.

			SCF	MBPT(2)	CCSD	CCSD(T)	B3LYP
		e	522	382	465	430(2.4)	453(2.9)
		e	841	558	659	584(6.7)	604(10.0)
N_4O	C_{3v}	a_1	834	710	772	730(1.1)	778(2.3)
		e	1173	762	932	845(15.2)	884(15.7)
		a_1	1378	912	1156	1059(1.8)	1149(1.1)
		a_1	1726	1703	1603	1579(344.7)	1657(347.3)
N_4O TS	C_s	a'		732i	683i	599i (38.8)	612i (49.1)
		a_u	251	224	228	222(2.2)	228(2.1)
		b_u	443	372	372	328(4.8)	343(4.2)
		a_g	575	558	519	486	498
		b_g	782	656	666	622	664
		a_g	805	690	714	702	725
N_4O_2	C_{2h}	a_g	894	908	898	870	876
		a_u	931	737	772	704(14.6)	743(19.5)
		b_u	969	866	853	789(93.6)	813(102.0)
		a_g	1260	1183	1130	1147	1133
		b_u	1450	1346	1356	1292(57.8)	1315(74.0)
		b_u	1931	1795	1726	1673(617.8)	1706(758.0)
		a_g	2217	1879	1935	1865	1904
N_4O_2 TS	C_s	a	1063i	1417i	1070i (73.4)		801i (23.5)
		a'	130	153	114	136(0.5)	148(0.5)
		a"	451	322	260	313(2.9)	318(1.0)
		a"	494	490	358	425(19.1)	493(5.1)
		a'	690	516	549	514(17.3)	532(19.2)
		a'	693	669	665	651(0.7)	674(1.0)
		a"	675	673	574	569(32.2)	573(24.7)
		a'	924	752	789	746(4.5)	774(2.6)
N_6O	C_s	a"	793	827	710	692(5.5)	711(7.3)
		a'	965	857	859	821(19.1)	835(30.4)
		a'	1167	1055	1091	1049(12.3)	1066(30.1)
		a'	1294	1138	1115	1073(23.7)	1091(2.0)
		a"	1493	1166	1266	1173(0.0)	1172(1.4)
		a"	1589	1262	1340	1257(11.6)	1284(23.6)
		a'	1715	1299	1440	1340(31.2)	1390(38.4)
		a'	1835	1717	1672	1609(201.6)	1648(269.0)
N_6O TS	C_1	a	882i	649i	511i	416i (51.5)	448i (52.9)

Table 3–6—continued.

			SCF	MBPT(2)	CCSD	CCSD(T)	B3LYP
		a_2	168	98	113	98	90
		b_1	194	145	149	141(0.4)	146(0.4)
		a_1	518	439	458	438(4.1)	445(2.9)
		b_1	569	462	482	453(16.0)	458(17.9)
		b_2	663	541	489	486(17.5)	536(13.4)
		a_1	672	591	600	578(1.7)	583(2.8)
		b_2	703	605	612	595(1.9)	606(33.3)
		b_2	811	706	643	616(48.8)	628(13.4)
N_6O_2	C_{2v}	a_2	868	714	747	709	738
		b_1	877	722	751	714(14.3)	745(18.2)
		a_1	861	768	754	713(2.2)	706(4.2)
		a_1	1092	1041	1010	992(11.8)	986(7.9)
		b_2	1249	1085	1088	1036(30.1)	1060(36.3)
		a_1	1443	1211	1259	1193(1.6)	1237(14.7)
		a_1	1484	1294	1295	1226(22.3)	1200(22.0)
		b_2	1664	1413	1451	1367(133.4)	1409(175.8)
		b_2	1812	1653	1628	1565(447.0)	1596(522.6)
		a_1	1909	1681	1702	1633(65.6)	1672(84.7)
N_6O_2 TS	C_s	a'	474i	541i	448i	446i (94.9)	319i (49.0)
		e"	166	131	131	127	128
		a_2"	236	207	206	201(3.3)	202(4.5)
		e'	512	442	456	442(7.6)	444(5.7)
		e'	633	575	572	552(12.9)	562(14.7)
		a_1'	791	674	697	662	679
		a_2'	822	628	648	602	690
N_6O_3	D_{3h}	a_2"	830	670	704	669(33.7)	695(38.6)
		e"	840	689	721	701	712
		a_1'	1038	988	956	938	943
		a_2'	1134	957	916	875	915
		e'	1252	1092	1102	1052(41.3)	1064(34.7)
		e'	1510	1364	1346	1283(175.0)	1271(218.4)
		e'	1788	1645	1610	1559(469.5)	1572(508.9)
		a_1'	1930	1687	1720	1660	1682
N_6O_3 TS	C_1	a	638i	364i	604i	420i (146.8)	293i (114.2)

3.7 Conclusions

In this work, we have quantitatively shown how four and six-membered nitrogen rings can be stabilized by coordinate covalent bonds to oxygen. Other potentially interesting coordinate covalent structures would include those to BH_3. Our analysis is based on locating the lowest energy transition state for unimolecular

dissociation. Although we believe we have done this effectively, we realize that with large molecules, and hence high-dimensional potential energy surfaces, other decomposition routes may exist. Similarly-transformed equation-of-motion (STEOM) calculations [71] of the vertical excitation energies at the singlet optimized geometries of N_4O_2 and N_6O_3 show the lowest triplet states to be at 60.4 and 56.1 kcal mol^{-1}, respectively. Since both of the triplets are high in energy, singlet-triplet crossings should not significantly lower the activation energies. In light of the stability characteristics of the N_2O dimer and trimer, the tetramer of N_2O might be expected to have similar properties. Our preliminary investigations show that N_8O_4 has a S_4-type structure. Although the smallest charge difference on adjacent nitrogens of the tetramer is 0.54 at the B3LYP level of theory, the structure is highly nonplanar. We have not investigated its transition states for unimolecular dissociation, and therefore cannot comment on its kinetic stability. All told, N_4O_2 and N_6O_3 are highly energetic molecules which appear to be stable. They are indeed worth attempts to synthesize. To facilitate their identification, we present harmonic infrared vibrational frequencies and their associated intensities in Table 3–6.

CHAPTER 4
HEATS OF FORMATION FOR THE AZACUBANES AND NITRO-SUBSTITUTED AZACUBANES

4.1 Introduction

The cubane system was first synthesized over 35 years ago by Eaton and Cole [118]. In light of cubane's immense strain energy (166 kcal mol^{-1}) and large positive heat of formation (148.7 kcal mol^{-1}), cubane's kinetic stability up to 230°C is quite unique [119,120]. This is in large part due to its highly symmetric structure which makes many of the dissociation pathways Woodward-Hoffman forbidden. Furthermore, appreciable geometry changes are only possible if two C–C bonds are broken simultaneously. Another feature of cubane's caged structure is its high density of 1.29 g cm^{-3} [120].

Based on their untypical structure and properties, cubane and its derivatives have emerged as outstanding candidates for high-energy density materials [21,24]. In fact, many of the nitrosubstituted cubanes have been prepared including octanitrocubane [121–124]. Since nitrogen is isoelectronic with -CH, some obvious derivatives are the azacubanes ($C_nN_{8-n}H_n$) and nitroazacubanes ($C_nN_{8-n}(NO_2)_n$). Chemical intuition based on the standard state of nitrogen suggests that the azacubanes will be higher in energy than the cubane parent molecule. However, intuition does not provide a means for estimating the magnitude of this energy difference. Since experimental data on the thermochemical properties of azacubanes is nonexistent (although one potential precursor has been made [125]) a theoretical investigation of these properties is warranted.

Estimating the relative stabilities of various azacubanes having a fixed number of nitrogen atoms (n) does not present a difficult theoretical problem since the gross

structural features of the possible isomers are similar, resulting in an approximate cancellation of errors in the electronic structure calculations. However, the energy difference between different classes of azacubanes (e.g. between the n=6 and n=4 isomers of $C_nN_{8-n}H_n$) is considerably more difficult to predict. Indeed, the most significant quantity to those interested in the potential use of azacubanes as fuels is the molar heat of formation (Δ H_f) defined by the enthalpy change in the reaction:

$$nH_2 + \frac{8-n}{2}N_2 + nC \longrightarrow C_nN_{8-n}H_n \qquad (4\text{–}1)$$

and a similar equation exists for the nitroazacubanes. Direct evaluation of ΔH_f by calculation of electronic energies for all species involved together with corrections for zero-point vibrational energies and temperature effects (with the latter contributions hereafter referred to as "thermodynamic corrections") is a notoriously difficult theoretical problem due to the different bonding situations present in the reactant and product sides of the chemical equation. For example, it has been demonstrated that calculation of the heat of formation of gaseous ammonia by direct calculation of NH_3, N_2, and H_2 produces results that can oscillate wildly with the level of theory and choice of basis set.

However, a procedure recommended by Pople and collaborators over three decades ago based on the use of isodesmic reactions [126, 127] provides a convenient means for determining heats of formation. An isodesmic reaction is defined as one in which the types of all chemical bonds are conserved in the course of the reaction. A trivial example of an isodesmic reaction is the conversion of the n=6 azacubane with nitrogens separated by the body diagonal to that in which the nitrogens are separated by a face diagonal. In both structures, there are 6 C– C single bonds, 6 C– N single bonds, and 4 C– H bonds. Interest in isodesmic reactions stems from the fact that the shortcomings of approximate wavefunctions and properties calculated from them are intrinsically related to the chemical environment of the

atoms making up a molecule. As a result of the structural similarities present on both sides of the equation, errors in absolute energies calculated for the species involved in an isodesmic reaction tend to cancel when the overall energy change for the reaction is calculated. Ideally, one chooses an isodesmic reaction where ΔH_f for all species except the one of interest have been accurately established experimentally. It is then a straightforward matter to calculate the heat of formation of the unknown species from a combination of the experimental results and the theoretical enthalpy change for the isodesmic process. Such an approach has been used with considerable success in the past to calculate heats of formation for a wide variety of molecules.

Nevertheless, the concept of chemical environment tacitly assumed in the preceding paragraph is oversimplified. For example, one might use the isodesmic reaction:

$$16CH_4 + C_8H_8 \longrightarrow 12C_2H_6 \tag{4–2}$$

together with experimental values for ethane and methane to estimate the heat of formation of cubane via the relation:

$$\Delta H_f(C_8H_8) = 12\Delta H_f(C_2H_6) - 16\Delta H_f(CH_4) - H_R \tag{4–3}$$

where H_R is the calculated enthalpy change for the isodesmic reaction. Note that while Equation 4–2 conforms to our definition of an isodesmic reaction (12 C– C bonds and 72 C– H bonds on both sides of the equation), it is clear that the C– C bonds in ethane are different from those in cubane, which is a highly strained system. Therefore, one should expect the approximate cancellation of errors in isodesmic reactions of this type to be less satisfactory than for processes such as:

$$C_3H_6 + CH_4 \longrightarrow C_2H_6 + C_2H_4 \tag{4–4}$$

Table 4–1. Naming conventions for the azacubanes and nitroazacubanes investigated in this study. The atomic positions are shown in Figure 4–1. For the azacubanes, the substituent of the carbon atom is hydrogen (X=H), and for the nitroazacubanes the substituent is a nitro group ($X=NO_2$).

Abbreviated Name	Formula	1	2	3	4	5	6	7	8
	$(CX)_8$	C	C	C	C	C	C	C	C
1-aza	$(CX)_7N$	N	C	C	C	C	C	C	C
1,3-diaza (trans)	$(CX)_6N_2$	N	C	N	C	C	C	C	C
1,8-diaza (opp)	$(CX)_6N_2$	N	C	C	C	C	C	C	N
1,2-diaza (cis)	$(CX)_6N_2$	N	N	C	C	C	C	C	C
1,3,5-triaza	$(CX)_5N_3$	N	C	N	C	N	C	C	C
1,2,5-triaza	$(CX)_5N_3$	N	N	C	C	N	C	C	C
1,2,3-triaza	$(CX)_5N_3$	N	N	N	C	C	C	C	C
1,3,5,7-tetraaza	$(CX)_4N_4$	N	C	N	C	N	C	N	C
1,2,3,5-tetraaza	$(CX)_4N_4$	N	N	N	C	N	C	C	C
1,2,5,8-tetraaza	$(CX)_4N_4$	N	N	C	C	N	C	C	N
1,2,3,7-tetraaza	$(CX)_4N_4$	N	N	N	C	C	C	N	C
1,2,3,6-tetraaza	$(CX)_4N_4$	N	N	N	C	C	N	C	C
1,2,3,4-tetraaza	$(CX)_4N_4$	N	N	N	N	C	C	C	C
1,2,3,5,7-pentaaza	$(CX)_3N_5$	N	N	N	C	N	C	N	C
1,2,3,5,6-pentaaza	$(CX)_3N_5$	N	N	N	C	N	N	C	C
1,2,3,4,5-pentaaza	$(CX)_3N_5$	N	N	N	N	N	C	C	C
1,2,3,4,5,7-hexaaza (trans)	$(CX)_2N_6$	N	N	N	N	N	C	N	C
1,2,3,5,6,8-hexaaza (opp)	$(CX)_2N_6$	N	N	N	C	N	N	C	N
1,2,3,4,5,6-hexaaza (cis)	$(CX)_2N_6$	N	N	N	N	N	N	C	C
1,2,3,4,5,6,7-septaaza	$(CX)N_7$	N	N	N	N	N	N	N	C
	N_8	N	N	N	N	N	N	N	N

which could be used to determine the heat of formation of propylene from known values for methane, ethane, and ethylene. A large volume of experience has demonstrated that enthalpy changes for isodesmic reactions of the latter variety can be calculated at even low levels of theory such as the self-consistent field (SCF) approximation with minimal or split-valence basis sets. However, for reactions such as Equation 4–2 in which the conserved "bond types" are less similar chemically, higher levels of theory should be used.

In this chapter, we apply isodesmic reaction strategies to study the absolute heats of formation for all isomers of the n=8 to n=0 azacubane and nitroazacubane

systems. Due to the strained nature of these systems and their unusual bonding environments, the considerations discussed above suggest that calculations based on a low-level *ab initio* approach may not be satisfactory. Hence, we have investigated the sensitivity of the predicted heats of formation by performing calculations at levels of sophistication ranging from the simple SCF model to coupled-cluster (CC) treatments that include effects of triple excitations. The purpose of the present study is threefold. In addition to providing what we believe to be accurate predictions for the formation enthalpies of the azacubanes and the nitroazacubanes beyond what is in the current literature [128–131], the systematic study of the dependence of ΔH_f as a function of the correlation treatment should provide some guidelines for investigations of related molecules. Finally, we compare the results obtained here with those predicted by semiempirical molecular orbital approaches and heats of formation computed directly from the standard states.

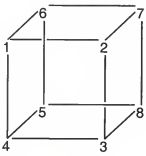

Figure 4–1. Numbering scheme used in this work.

Table 4–2. Model compounds for isodesmic reactions and their experimental heats of formation in kcal mol^{-1} [114].

molecule	ΔH_f
CH_4	-17.9
CH_3NH_2	-5.4
CH_3NO_2	-19.3
C_2H_6	-20.0
NH_3	-11.0
$N(CH_3)_3$	-5.7
N_2H_4	22.8

4.2 Methods

The first step in calculating the heat of formation is to determine an isodesmic reaction for each molecule. A small number of simple molecules were chosen as sources of different types of bonds. For example, for a C– C single bond, ethane was used. For a N– C single bond, methyl amine was used. All of the model compounds are listed in Table 4–2 along with their experimental heats of formation. The sole restriction is that only molecules with experimentally known heats of formation in the ideal gas state may be used. This set of molecules was used to form balanced chemical reactions where both the individual atoms and the number of each type of bond were balanced. Isodesmic reactions for the azacubanes and nitroazacubanes are given in Tables 4–3 and 4–6, respectively. One consequence of the large stoichiometric coefficients is that small errors in the computed energy for each model compound are multiplied by large numbers.

In this study, CC calculations were done with the ACES II package [68]. The semi-empirical and DFT calculations were performed with the GAUSSIAN 94 package [132]. The calculations were done using the Dunning double ζ (DZ) basis set [133, 134] with polarization functions from correlated calculations [135]. The geometries for all molecules were optimized at the SCF level and are available upon request to interested parties. Using these geometries, the energies were calculated at the AM1 [136], MINDO3 [137], PM3 [138], BLYP, B3LYP, SCF, MBPT(2), CCSD, and CCSD(T) [139] levels. Pure spherical harmonics (i.e., 5 d-type functions) were used and all core electrons were omitted from the correlation procedure. We did not perform CCSD and CCSD(T) calculations for the series of nitroazacubanes.

Frequency calculations were also done at the SCF level, and the frequencies obtained were used to verify the existence of a structure with no imaginary frequencies. Moreover, the computed frequencies were used to calculate the zero-point vibrational energy as well as the thermodynamic corrections for

Table 4–3. Reaction coefficients for the isodesmic reaction: azacubane + α CH_4 + β NH_3 $\rightarrow$ γ N_2H_4 + δ CH_3NH_2 + ϵ C_2H_6

azacubane	α	β	γ	δ	ϵ
$(CH)_8$	0	16	0	0	12
1-aza	2	14	0	3	9
1,3-diaza (trans)	4	12	0	6	6
1,8-diaza (opp)	4	12	0	6	6
1,2-diaza (cis)	4	12	1	4	7
1,3,5-triaza	6	10	0	9	3
1,2,5-triaza	6	10	1	7	4
1,2,3-triaza	6	10	2	5	5
1,3,5,7-tetraaza	8	8	0	12	0
1,2,3,5-tetraaza	8	8	2	8	2
1,2,5,8-tetraaza	8	8	2	8	2
1,2,3,7-tetraaza	8	8	3	6	3
1,2,3,6-tetraaza	8	8	3	6	3
1,2,3,4-tetraaza	8	8	4	4	4
1,2,3,5,7-pentaaza	10	6	3	9	0
1,2,3,5,6-pentaaza	10	6	4	7	1
1,2,3,4,5-pentaaza	10	6	5	5	2
1,2,3,4,5,7-hexaaza (trans)	12	4	6	6	0
1,2,3,5,6,8-hexaaza (opp)	12	4	6	6	0
1,2,3,4,5,6-hexaaza (cis)	12	4	7	4	1
1,2,3,4,5,6,7-heptaaza	14	2	9	3	0
N_8	16	0	12	0	0

finite-temperature. Given this data, the heats of formation for each of the azacubanes and nitroazacubanes were determined.

Heats of formation were also computed directly from the standard states of the elements. Again, this is an extremely demanding test for a theoretical method as nearly every bond in the molecule is broken. To correct for the standard state of carbon, we used the experimental heat of formation of 169.9 kcal mol^{-1} for the ^3P state [114].

4.3 Results and Discussion

The heats of formation for the series of azacubanes are presented in Table 4–4. The series is arranged in terms of increasing nitrogen content and for the

Table 4–4. Heats of formation in kcal mol^{-1} for the azacubanes.

azacubane	AM1	MINDO3	PM3	BLYP	B3LYP	SCF	MBPT(2)	CCSD	CCSD(T)	exp
$(CH)_8$	233.4	277.6	141.4	131.9	142.8	160.5	148.8	153.4	150.4	148.7 [140], 159 [141]
1-aza	275.5	262.9	170.2	150.3	161.2	178.5	163.9	168.6	165.2	
1,3-diaza(trans)	321.3	244.0	201.2	168.2	178.7	194.8	177.6	182.5	178.7	
1,8-diaza(opp)	319.7	248.5	199.3	170.3	181.2	198.4	180.7	185.5	181.6	
1,2-diaza(cis)	329.6	256.1	210.1	184.1	195.4	213.3	195.2	199.8	195.8	
1,3,5-triaza	371.2	220.6	234.5	185.5	195.4	209.7	190.0	195.4	191.2	
1,2,5-triaza	377.6	237.4	241.5	203.2	214.4	231.4	210.3	215.3	210.8	
1,2,3-triaza	385.9	245.4	250.8	216.5	228.2	245.9	224.3	229.1	224.4	
1,3,5,7-tetraaza	425.8	192.7	270.4	202.3	211.4	223.7	201.7	207.6	203.0	
1,2,3,5-tetraaza	438.0	222.2	284.8	235.1	246.3	262.7	238.2	243.4	238.3	
1,2,5,8-tetraaza	438.0	227.4	284.3	237.6	249.1	266.3	241.5	246.6	241.4	
1,2,3,7-tetraaza	444.7	230.8	292.5	248.0	259.7	276.8	251.7	256.8	251.5	
1,2,3,6-tetraaza	444.1	235.1	292.1	250.5	262.5	280.4	255.1	260.0	254.7	
1,2,3,4-tetraaza	450.4	242.3	300.1	264.6	277.0	295.8	270.1	275.0	269.6	
1,2,3,5,7-pentaaza	501.3	202.7	329.2	266.0	277.2	292.6	264.5	270.2	264.4	
1,2,3,5,6-pentaaza	506.9	220.7	336.1	283.7	295.9	313.6	284.5	289.7	283.7	
1,2,3,4,5-pentaaza	511.5	228.1	342.4	297.4	310.1	328.5	299.1	304.2	298.1	
1,2,3,4,5,7-hexaaza	577.4	209.2	387.8	329.5	342.4	360.2	326.7	332.4	325.5	
1,2,3,5,6,8-hexaaza	578.6	215.2	389.0	331.4	344.4	362.9	329.2	334.4	327.5	
1,2,3,4,5,6-hexaaza	581.4	222.1	393.5	345.8	359.3	378.3	344.7	350.0	343.0	
1,2,3,4,5,6,7-septaaza	654.8	211.8	446.5	393.1	407.3	426.8	388.4	394.1	386.2	
N_8	734.1	209.9	505.6	456.2	471.6	492.4	449.1	455.1	446.2	

azacubanes with the same chemical formula, increasing N– N bonds. For cubane, there are two experimental values of its heat of formation. In 1966, a value of 148.7 kcal mol^{-1} was obtained directly from cubane [140]. A more recent value of 159 kcal mol^{-1} was estimated indirectly from the heat of combustion of 1,4-bis(methoxycarbonyl)cubane [141]. Our most reliable CCSD(T) estimate of 150.4 kcal mol^{-1} is more consistent with the older, direct measurement. Trends in the ΔH_f values for different methods are better presented graphically in Figure 4–2. Here, the AM1 and MINDO3 methods show large variations from all of the other methods. However, PM3, the other semiempirical method, is closer to the *ab initio* methods. Figure 4–3 offers a magnified view, where ΔH_f differences with respect to CCSD(T) are plotted. The BLYP and B3LYP values show the same trend with large variations along the series. The MBPT(2) and CCSD results more closely follow the CCSD(T) values for the range of molecules studied.

Another important trend along the series of azacubanes is the energy change in the isodesmic reactions. The isodesmic reaction energies for the various methods are presented in Table 4–5 and graphically in Figure 4–4. In the bond energy additivity model where the energy of a molecule is approximated by the sum of its bond energies, these values would be zero as they represent strain, resonance stabilization, and other effects. For nearly all of the azacubanes, $-\Delta E_{isodesmic}$ is greater than zero suggesting that they are less stable than their molecular fragments. However, $-\Delta E_{isodesmic}$ does decrease along the series with increasing nitrogen content. Beginning with cubane, $-\Delta E_{isodesmic}$ is 104.6 kcal mol^{-1} from CCSD(T) and decreases to -2.8 kcal mol^{-1} for N_8. This trend is consistent with an earlier investigation which showed that introduction of nitrogen into the cube stabilizes it by σ-conjugation of the lone pairs [142]. Also, since nitrogen prefers angles slightly less than 109.5 degrees as opposed to carbon, more substituted cubes

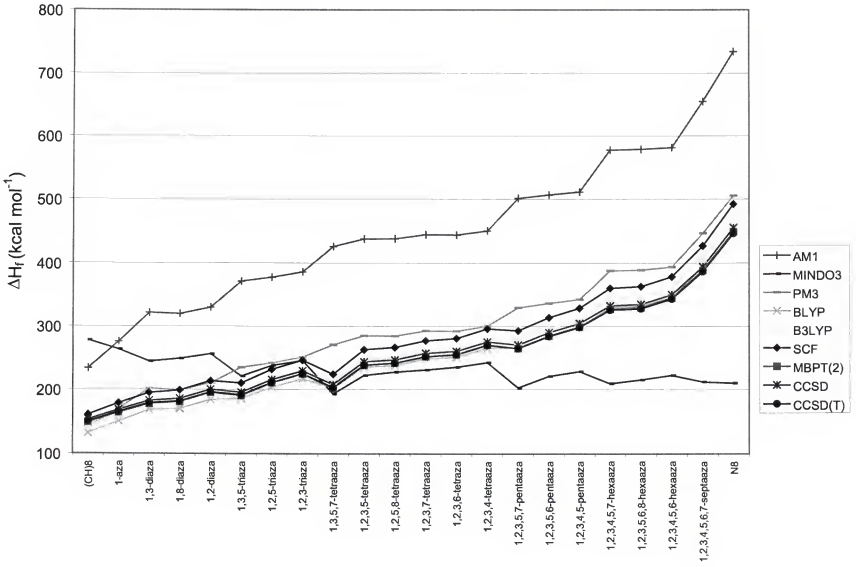

Figure 4–2. ΔH_f for the azacubanes.

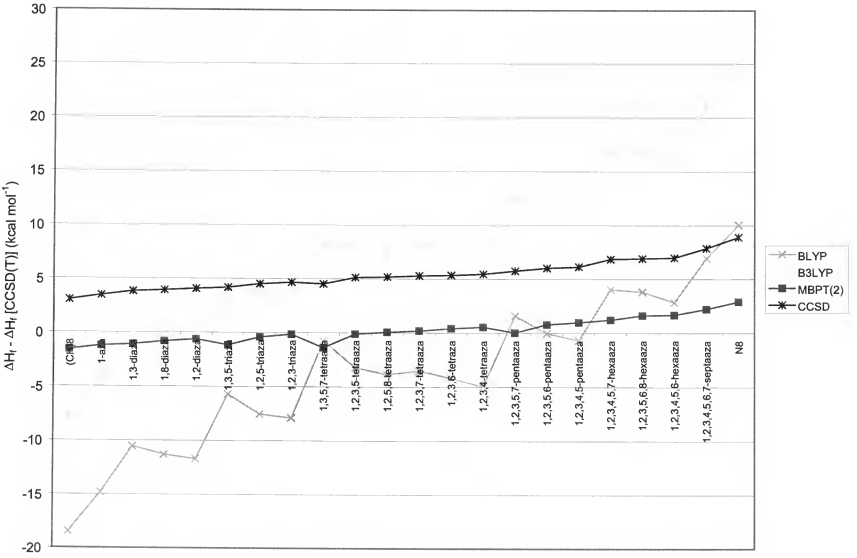

Figure 4–3. ΔH_f relative to CCSD(T) for the azacubanes.

Table 4–5. $-\Delta E_{isodesmic}$ in kcal mol^{-1} for the azacubanes.

azacubane	AM1	MINDO3	PM3	BLYP	B3LYP	SCF	MBPT(2)	CCSD	CCSD(T)
$(CH)_8$	187.6	231.7	95.6	86.1	97.0	114.7	103.0	107.6	104.6
1-aza	199.5	187.0	94.3	74.4	85.2	102.5	87.9	92.6	89.2
1,3-diaza (trans)	215.2	137.9	95.1	62.1	72.6	88.7	71.5	76.4	72.6
1,8-diaza (opp)	213.6	142.4	93.2	64.2	75.1	92.3	74.6	79.4	75.5
1,2-diaza (cis)	210.0	136.4	90.5	64.5	75.8	93.7	75.5	80.2	76.2
1,3,5-triaza	235.0	84.3	98.2	49.3	59.1	73.4	53.8	59.1	55.0
1,2,5-triaza	227.9	87.7	91.7	53.5	64.6	81.6	60.6	65.5	61.0
1,2,3-triaza	222.6	82.1	87.6	53.3	64.9	82.7	61.0	65.9	61.2
1,3,5,7-tetraaza	259.4	26.3	104.0	35.9	45.0	57.3	35.3	41.2	36.7
1,2,3,5-tetraaza	244.6	28.8	91.4	41.7	52.9	69.3	44.8	50.0	44.9
1,2,3,5-tetraaza	244.6	34.0	90.9	44.2	55.7	72.9	48.1	53.2	48.0
1,2,5,8-tetraaza	237.8	23.9	85.6	41.1	52.8	69.9	44.8	49.9	44.6
1,2,3,7-tetraaza	237.2	28.2	85.2	43.6	55.6	73.5	48.2	53.1	47.8
1,2,3,6-tetraaza	230.0	21.9	79.7	44.2	56.6	75.4	49.7	54.6	49.2
1,2,3,5,7-pentaaza	264.3	-34.3	92.1	29.0	40.2	55.6	27.4	33.2	27.4
1,2,3,5,6-pentaaza	256.4	-29.9	85.6	33.1	45.4	63.0	34.0	39.2	33.2
1,2,3,4,5-pentaaza	247.4	-35.9	78.3	33.3	46.0	64.4	35.0	40.2	34.0
1,2,3,4,5,7-hexaaza (trans)	269.7	-98.5	80.2	21.8	34.7	52.5	19.0	24.7	17.8
1,2,3,5,6,8-hexaaza (opp)	270.9	-92.5	81.3	23.6	36.7	55.2	21.5	26.8	19.8
1,2,3,4,5,6-hexaaza (cis)	260.2	-99.0	72.3	24.6	38.1	57.1	23.5	28.8	21.8
1,2,3,4,5,6,7-septaaza	276.4	-166.6	68.2	14.8	29.0	48.4	10.1	15.7	7.8
N_8	285.1	-239.1	56.6	7.2	22.6	43.4	0.1	6.1	-2.8

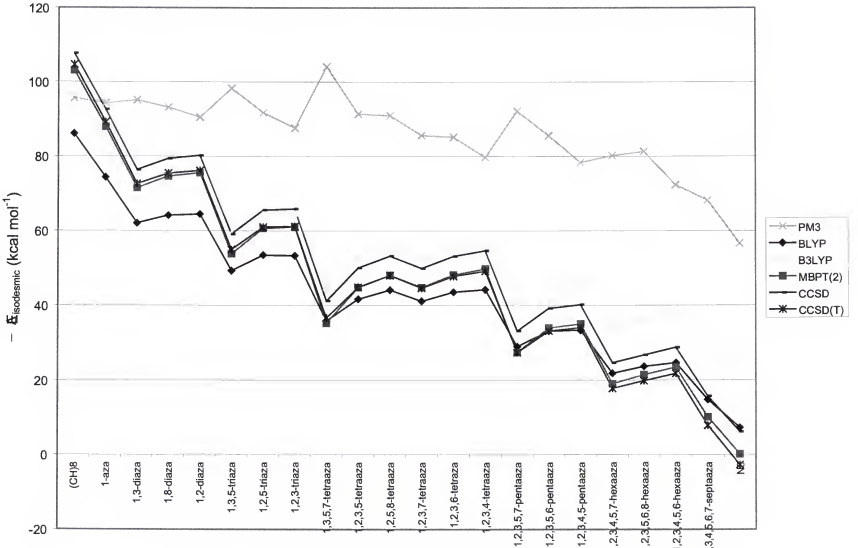

Figure 4–4. -$\Delta E_{isodesmic}$ for the azacubane.

have lower strain energies. On this scale, the PM3 values show large variations with respect to all other methods.

Figure 4–5 presents the $\Delta E_{isodesmic}$ trends relative to CCSD(T). Again, the BLYP and B3LYP results show large variations over the series, while the MBPT(2) and CCSD results are more consistent. The range of the BLYP and B3LYP values are 27.4 and 33, respectively, while the MBPT(2) and CCSD methods have a much smaller range of 4.5 and 7 kcal mol^{-1}, respectively. The largest difference for the DFT methods is for N_8, where B3LYP differs from the CCSD(T) result by 25.4 kcal mol^{-1}.

Table 4–6. Reaction coefficients for the isodesmic reaction: nitroazacubane + α CH_4 + β NH_3 → γ N_2H_4 + δ CH_3NO_2 + ϵ C_2H_6 + ζ $N(CH_3)_3$

nitroazacubane	α	β	γ	δ	ϵ	ζ
$(CNO_2)_8$	24	0	0	8	12	0
1-aza	21	0	0	7	9	1
1,3-diaza (trans)	18	$\frac{4}{3}$	1	6	7	$\frac{4}{3}$
1,8-diaza (opp)	18	$\frac{4}{3}$	1	6	7	$\frac{4}{3}$
1,2-diaza (cis)	18	$\frac{4}{3}$	1	6	7	$\frac{4}{3}$
1,3,5-triaza	15	0	0	5	3	3
1,2,5-triaza	15	$\frac{4}{3}$	1	5	4	$\frac{7}{3}$
1,2,3-triaza	15	$\frac{8}{3}$	2	5	5	$\frac{5}{3}$
1,3,5,7-tetraaza	12	0	0	4	0	4
1,2,3,5-tetraaza	12	$\frac{8}{3}$	2	4	2	$\frac{8}{3}$
1,2,5,8-tetraaza	12	4	3	4	3	2
1,2,3,7-tetraaza	12	$\frac{8}{3}$	2	4	2	$\frac{8}{3}$
1,2,3,6-tetraaza	12	4	3	4	3	2
1,2,3,4-tetraaza	12	$\frac{16}{3}$	4	4	4	$\frac{4}{3}$
1,2,3,5,7-pentaaza	9	4	3	3	0	3
1,2,3,5,6-pentaaza	9	$\frac{16}{3}$	4	3	1	$\frac{7}{3}$
1,2,3,4,5-pentaaza	9	$\frac{20}{3}$	5	3	2	$\frac{5}{3}$
1,2,3,4,5,7-hexaaza (trans)	6	8	6	2	0	2
1,2,3,5,6,8-hexaaza (opp)	6	8	6	2	0	2
1,2,3,4,5,6-hexaaza (cis)	6	$\frac{28}{3}$	7	2	1	$\frac{4}{3}$
1,2,3,4,5,6,7-septaaza	3	12	9	1	0	1
N_8	0	16	12	0	0	0

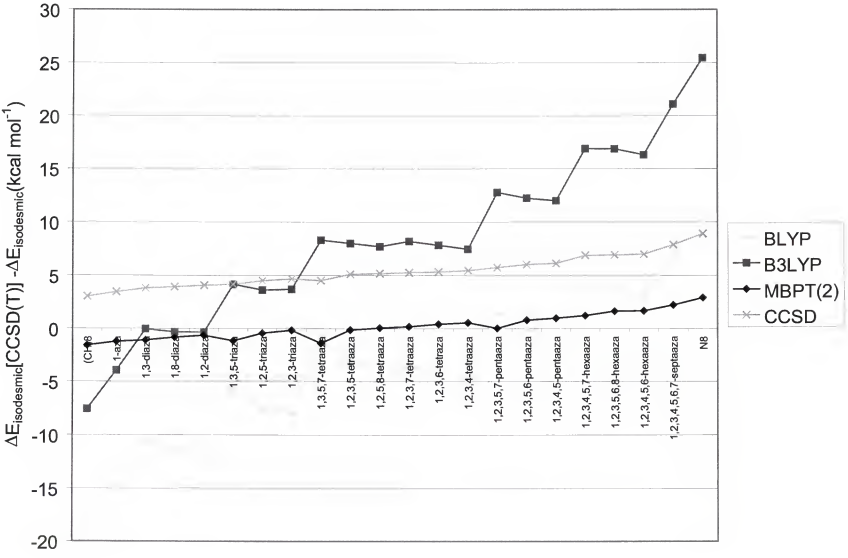

Figure 4–5. -$\Delta E_{isodesmic}$ relative to CCSD(T) for the azacubanes.

Table 4–7. Heats of formation in kcal mol^{-1} for the nitroazacubanes.

nitroazacubane	AM1	MINDO3	PM3	BLYP	B3LYP	SCF	MBPT(2)
$(CNO_2)_8$	333.2	172.5	165.5	138.7	163.6	230.2	126.6
1-aza	359.1	-32.2	39.6	151.8	175.0	233.0	148.1
1,3-diaza (trans)	396.3	115.7	238.1	170.1	191.2	240.0	147.4
1,8-diaza (opp)	396.0	129.2	246.0	170.1	191.6	241.0	149.1
1,2-diaza (cis)	399.2	-124.2	0.3	185.8	208.4	260.7	187.5
1,3,5-triaza	417.9	-609.4	-377.0	180.4	199.8	239.9	187.9
1,2,5-triaza	428.8	-227.1	-26.4	199.6	220.6	264.7	207.5
1,2,3-triaza	442.6	-189.6	-10.8	220.8	239.0	284.8	222.4
1,3,5,7-tetraaza	452.2	-269.1	47.4	193.1	210.2	241.1	204.1
1,2,3,5-tetraaza	474.7	-187.5	70.0	231.2	250.8	288.4	240.5
1,2,5,8-tetraaza	483.6	-151.0	71.5	238.2	257.9	296.0	244.5
1,2,3,7-tetraaza	477.1	-183.9	73.9	244.9	265.8	306.6	257.5
1,2,3,6-tetraaza	488.3	-151.4	82.3	247.6	267.5	306.7	254.0
1,2,3,4-tetraaza	497.9	-111.7	93.6	267.4	288.2	330.3	230.5
1,2,3,5,7-pentaaza	523.1	-150.2	164.4	260.1	277.9	308.4	269.0
1,2,3,5,6-pentaaza	533.2	-107.4	174.5	281.6	300.8	334.7	290.5
1,2,3,4,5-pentaaza	544.0	-73.1	183.5	297.1	316.6	352.0	303.5
1,2,3,4,5,7-hexaaza (trans)	593.5	-30.9	280.1	326.6	344.4	373.2	332.1
1,2,3,5,6,8-hexaaza (opp)	593.7	-26.5	281.3	330.6	348.9	378.5	337.4
1,2,3,4,5,6-hexaaza (cis)	602.6	10.2	288.5	345.8	364.2	395.0	350.2
1,2,3,4,5,6,7-septaaza	663.8	89.0	393.9	392.3	409.2	434.6	392.4
N_8	734.1	209.9	505.6	456.2	471.6	492.4	449.1

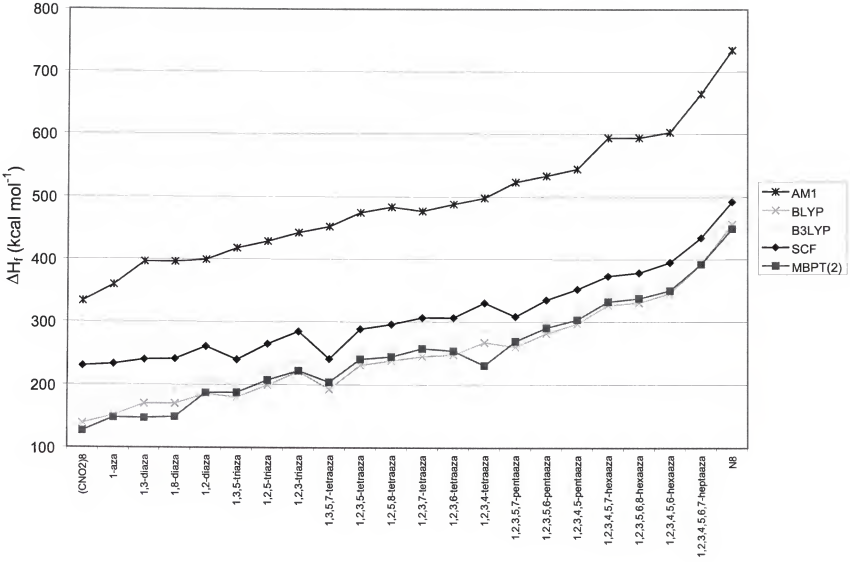

Figure 4–6. ΔH_f for the nitroazacubanes.

For the nitroazacubanes, the heats of formation are presented in Table 4–7 and graphically in Figure 4–6. Beginning with octanitrocubane, ΔH_f's progressively increase along the series with increasing nitrogen content of the cube. When compared to the azacubanes, the difference in the MBPT(2) and SCF values is much larger due to the presence of more nitrogen atoms with lone electron pairs. Differences in ΔH_f relative to MBPT(2) are presented in Figure 4–7. All three of the models (SCF, BLYP, and B3LYP) display the same trend with large variations over the series. One interesting aspect in the energies is the orientation and repulsion of NO_2 groups. All structures have been fully optimized and have no imaginary frequencies at the SCF level of theory. Although there is a low barrier for rotation of a NO_2 group, the repulsion of adjacent nitro groups would involve a much higher energy. For 1,2,3,4-tetraaza, there is a large uncharacteristic difference in the methods with respect to MBPT(2), apparently due to the difficulty in describing the repulsion of adjacent nitro groups.

The isodesmic reaction energies for the nitroazacubanes are presented in Table 4–8 and graphically in Figure 4–8. Again, $-E_{isodesmic}$ decreases along the series with increasing nitrogen content of the cube. In fact, the $E_{isodesmic}$ values for the nitroazacubanes are very close to those for the azacubanes. Another aspect of the nitroazacubane energies, however is the orientation and repulsion of the $-NO_2$ groups. There is a small peak in the isodesmic reaction energies for the molecule 1,2,3,7-tetraaza. Although not all of the nitro groups are attached to the same face of the cube (see Figure 4–1), this structure seems to have a large amount of repulsion.

Heats of formation were also computed directly from the standard states of the elements. The values for the azacubanes are presented in Table 4–9 and those for the nitroazacubanes are presented in Table 4–10. The differences of the direct values with respect to the most accurate isodesmic method are presented in Figures

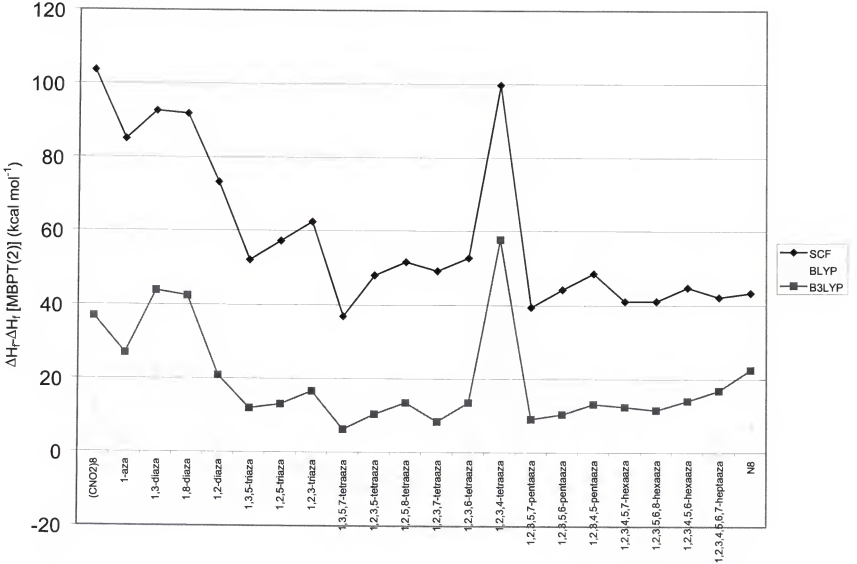

Figure 4–7. ΔH_f relative to MBPT(2) for the nitroazacubanes.

Table 4–8. -$\Delta E_{isodesmic}$ in kcal mol^{-1} for the nitroazacubanes.

nitroazacubane	AM1	BLYP	B3LYP	SCF	MBPT(2)
$(CNO_2)_8$	298.6	104.2	129.1	195.7	92.2
1-aza	304.5	97.2	120.4	178.4	93.5
1,3-diaza (trans)	300.4	74.3	95.4	144.2	72.8
1,8-diaza (opp)	300.2	74.3	95.8	145.2	74.5
1,2-diaza (cis)	303.4	90.0	112.6	164.9	91.7
1,3,5-triaza	323.1	85.6	105.1	145.2	93.2
1,2,5-triaza	312.9	83.7	104.7	148.8	91.6
1,2,3-triaza	305.6	83.7	102.0	147.7	85.4
1,3,5,7-tetraaza	337.4	78.3	95.4	126.2	89.3
1,2,3,5-tetraaza	317.5	74.1	93.6	131.3	83.3
1,2,5,8-tetraaza	305.3	59.9	79.6	117.7	66.2
1,2,3,7-tetraaza	319.9	87.8	108.7	149.5	100.4
1,2,3,6-tetraaza	310.0	69.3	89.2	128.4	75.8
1,2,3,4-tetraaza	298.4	67.9	88.7	130.8	73.2
1,2,3,5,7-pentaaza	324.7	61.7	79.6	110.0	70.6
1,2,3,5,6-pentaaza	313.6	62.0	81.2	115.2	71.0
1,2,3,4,5-pentaaza	303.4	56.4	75.9	111.3	62.8
1,2,3,4,5,7-hexaaza (trans)	311.6	44.7	62.5	91.2	50.2
1,2,3,5,6,8-hexaaza (opp)	311.8	48.7	67.0	96.6	55.5
1,2,3,4,5,6-hexaaza (cis)	299.6	42.7	61.1	91.9	47.1
1,2,3,4,5,6,7-septaaza	298.3	26.8	43.8	69.2	27.0
N_8	285.1	7.2	22.6	43.4	0.1

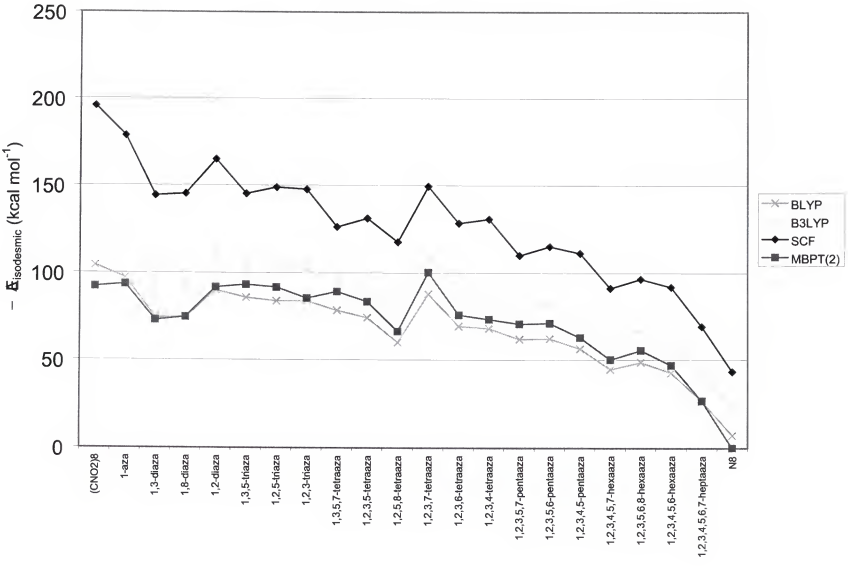

Figure 4–8. -$\Delta E_{isodesmic}$ for the nitroazacubanes.

Table 4–9. Heats of formation in kcal mol^{-1} for the nitroazacubanes computed directly.

azacubane	PM3	BLYP	B3LYP	MBPT(2)
$(CNO_2)_8$	205.1	162.7	181.0	181.7
1-aza	203.4	171.6	187.4	193.4
1,3-diaza (trans)	204.0	179.9	193.0	203.7
1,8-diaza (opp)	202.0	182.0	195.6	206.8
1,2-diaza (cis)	215.1	194.4	208.5	220.9
1,3,5-triaza	206.8	187.7	197.8	212.7
1,2,5-triaza	216.0	204.0	215.5	232.7
1,2,3-triaza	227.6	215.9	228.0	246.3
1,3,5,7-tetraaza	212.2	194.9	201.8	220.9
1,2,3,5-tetraaza	231.1	224.9	234.2	256.8
1,2,5,8-tetraaza	230.7	227.3	237.0	260.1
1,2,3,7-tetraaza	241.1	236.4	246.4	270.0
1,2,3,6-tetraaza	240.7	238.8	249.2	273.4
1,2,3,4-tetraaza	251.0	251.6	262.5	288.1
1,2,3,5,7-pentaaza	247.3	244.9	252.0	279.4
1,2,3,5,6-pentaaza	256.5	261.1	269.4	299.1
1,2,3,4,5-pentaaza	265.0	273.4	282.3	313.4
1,2,3,4,5,7-hexaaza (trans)	282.3	294.6	301.4	337.3
1,2,3,5,6,8-hexaaza (opp)	283.4	296.4	303.5	339.7
1,2,3,4,5,6-hexaaza (cis)	290.3	309.4	317.1	354.9
1,2,3,4,5,6,7-septaaza	317.3	344.3	350.7	394.6
N_8	352.8	393.6	399.3	451.0

4–9 and 4–10 for the azacubanes and nitroazacubanes, respectively. All methods vary over a large range and the accurate description of ΔH_f directly seems to be beyond the current limits of *ab initio* correlated methods. Thus, calculation of heats of formation directly from the elements is not the preferable route.

4.4 Conclusions

Although a caged structure might be difficult to achieve synthetically, molecules of this type have some of the highest densities. Octanitrocubane's density has been estimated as 1.985 g cm^{-3} [143]. All of the azacubanes and the nitroazacubanes are highly energetic molecules. With increasing nitrogen content, greater heats of formation are achieved as well as more stable structures with

Table 4–10. $-\Delta E_{isodesmic}$ in kcal mol^{-1} for the nitroazacubanes computed directly.

nitroazacubane	PM3	BLYP	B3LYP	MBPT(2)
$(CNO_2)_8$	172.2	153.5	207.9	168.0
1-aza	178.4	163.0	210.2	184.0
1,3-diaza(trans)	188.2	173.7	213.7	199.5
1,8-diaza(opp)	183.0	173.7	214.1	201.2
1,2-diaza(cis)	196.1	189.4	230.8	218.4
1,3,5-triaza	200.0	184.5	216.9	213.1
1,2,5-triaza	204.3	199.7	234.0	233.0
1,2,3-triaza	215.6	216.8	248.8	248.2
1,3,5,7-tetraaza	215.6	193.7	218.3	223.9
1,2,3,5-tetraaza	229.3	223.6	251.4	260.9
1,2,5,8-tetraaza	226.4	226.6	254.9	265.2
1,2,3,7-tetraaza	233.3	237.3	266.5	277.9
1,2,3,6-tetraaza	237.2	235.9	264.5	274.8
1,2,3,4-tetraaza	244.1	251.6	281.5	293.7
1,2,3,5,7-pentaaza	252.3	244.9	265.9	284.3
1,2,3,5,6-pentaaza	258.0	262.3	285.0	306.1
1,2,3,4,5-pentaaza	262.6	273.8	297.2	319.4
1,2,3,4,5,7-hexaaza(trans)	287.8	295.6	312.3	342.9
1,2,3,5,6,8-hexaaza(opp)	288.9	299.6	316.7	348.3
1,2,3,4,5,6-hexaaza(cis)	291.7	310.7	328.4	361.3
1,2,3,4,5,6,7-septaaza	321.3	345.5	357.0	398.8
N_8	352.8	393.7	399.3	450.9

respect to fragments of the isodesmic reaction. Semi-empirical methods are inadequate for this problem, though PM3 is better than the others. Reparameterized semi-empirical theory as manifested in the transfer Hamiltonian might be able to overcome these limitations [144].

Although N_8 is too unstable for production in bulk quantities, molecules within the azacubane and nitroazacubane series might offer more kinetic stability, albeit a lower heat of formation. Some estimates of decomposition pathways and energy barriers for the azacubanes have been made [15, 145].

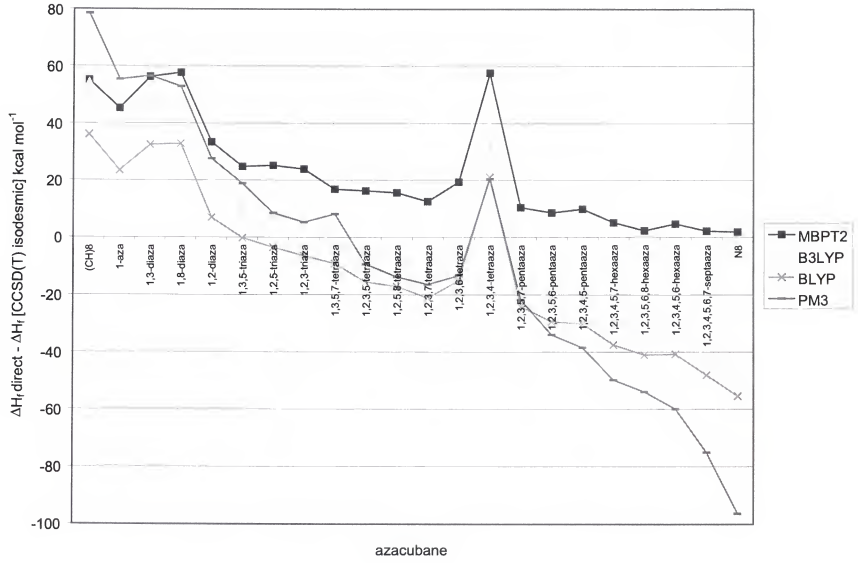

Figure 4–9. ΔH_f from direct calculations relative to ΔH_f from CCSD(T) isodesmic route.

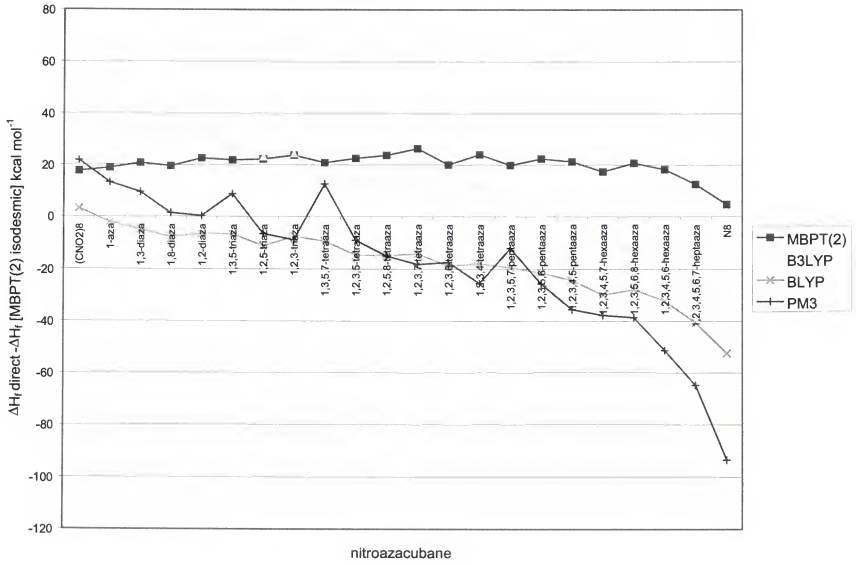

Figure 4–10. ΔH_f from direct calculations relative to ΔH_f from MBPT(2) isodesmic route.

CHAPTER 5
CHOICES FOR THE ORBITAL SPACE

One of the major limitations for quantum chemical calculations is the dimension of the molecular orbital basis. In fact, the computational cost for *ab initio* correlated methods has a tremendous dependence on the size of the molecular orbital basis. Despite many chemically-interesting processes, it is prohibitively expensive to describe systems with more than about 10 first-row atoms or about 300 molecular orbitals using highly correlated methods.

Typically, molecular orbitals are defined from canonical Hartree-Fock (HF) theory. Although, the HF determinant has the lowest energy as an expectation value of a single Slater determinant with the Hamiltonian, the excited or 'virtual' orbitals are purely a by-product of the HF calculation in a basis set,[a] so they are not necessarily the best set for correlated calculations. In this chapter, we review the merits of Hartree-Fock theory, and provide alternate choices for molecular orbitals.

5.1 SCF Orbitals

In Hartree-Fock theory [146], the exact Hamiltonian is approximated by a sum of one-electron Fock operators

$$\mathcal{H} = \sum_i h(i) + \sum_{i<j} r_{ij}^{-1} + \sum_{\alpha<\beta} \frac{Z_\alpha Z_\beta}{R_{\alpha\beta}} \approx \sum_i^n \mathcal{F}(i) + E_{\text{nuclear repulsion}} \tag{5–1}$$

$$\mathcal{F}(i) = h(i) + v^{eff}(i) \tag{5–2}$$

[a] For atomic and diatomic systems, it is possible to solve the Hartree-Fock equations numerically, rather than in a finite set of Slater- or Gaussian-type functions. In these numerical solutions, virtual orbitals are not defined.

The set of orbitals, $\{\varphi_n\}$, are optimized to give the lowest electronic energy while remaining orthonormal. Such conditions are imposed using Lagrange multipliers and functional derivatives.

$$\mathcal{L}\left[\{\varphi_n\}\right] = E_0\left[\{\varphi_n\}\right] - \sum_{ij} \lambda_{ij}\left(\langle i|j\rangle - \delta_{ij}\right) \tag{5–3}$$

Since $\mathcal{L}$ is real and $\langle i|j\rangle^* = \langle j|i\rangle$, the multipliers constitute an Hermitian matrix.

$$\lambda_{ji}^* = \lambda_{ij} \tag{5–4}$$

Taking the partial derivative of $\mathcal{L}$ with respect to φ_k^* yields:

$$\frac{\delta\mathcal{L}}{\delta\varphi_k^*} = \langle\delta\varphi_k|h|\varphi_k\rangle + \frac{1}{2}\sum_j \langle\delta\varphi_k\varphi_j||\varphi_k\varphi_j\rangle + \frac{1}{2}\sum_i \langle\varphi_i\delta\varphi_k||\varphi_i\varphi_k\rangle - \sum_j \lambda_{kj}\langle\delta\varphi_k|\varphi_j\rangle \tag{5–5}$$

Setting Equation 5–5 equal to zero, factoring $\delta\varphi_k$ from every term, and combining the summation indices gives:

$$h|\varphi_k\rangle + \left[\sum_j \left(\hat{J}_j - \hat{K}_j\right)\right]|\varphi_k\rangle - \sum_j \lambda_{kj}|\varphi_j\rangle = 0 \tag{5–6}$$

where $\hat{J}$ and $\hat{K}$ have been introduced to denote the Coulomb and exchange operators, respectively. Because $v^{eff} = \sum_j \left(\hat{J}_j - \hat{K}_j\right)$, Equation 5–6 is a pseudo-eigenvalue equation in terms of the Fock operator. It is often beneficial to diagonalize the $\boldsymbol{\lambda}$ matrix to provide an energy for each orbital.

$$\boldsymbol{\epsilon} = \boldsymbol{U}^\dagger\boldsymbol{\lambda}\boldsymbol{U} \tag{5–7}$$

However, there are several considerations to obtaining orbital energies. The first is whether expectation values will differ between the two wave functions. If λ is diagonalized by a real unitary matrix $\left(\mathbf{U}^\dagger = \mathbf{U}^{-1}; \mathbf{U}^\dagger\mathbf{U} = \mathbf{1}\right)$, the new wave function can be written in terms of the old one as

$$|\Psi'\rangle = det(\mathbf{U})|\Psi\rangle \tag{5–8}$$

and the expectation values as

$$\langle \Psi' | \hat{A} | \Psi' \rangle = det\left(\mathbf{U}^{\dagger}\mathbf{U}\right) \langle \Psi | \hat{A} | \Psi \rangle = det\left(\mathbf{1}\right) \langle \Psi | \hat{A} | \Psi \rangle \tag{5-9}$$

Hence, all expectation values will be invariant to unitary transformations of the wave function. The second question is whether the Fock operator is invariant. The only part of the Fock operator that depends on the orbitals is v^{eff} and it is considered below:

$$\begin{aligned} v^{eff\prime}(1) &= \sum_j \int \varphi_j^{*\prime}(2) \frac{1 - P_{12}}{r_{12}} \varphi_j^{\prime}(2) d\tau_2 \\ &= \sum_j \int \sum_k \left(U^{\dagger}\right)_{jk} \varphi_k^*(2) \frac{1 - P_{12}}{r_{12}} \sum_l U_{lj} \varphi_l(2) d\tau_2 \\ &= \sum_{kl} \int \delta_{kl} \varphi_k^*(2) \frac{1 - P_{12}}{r_{12}} \varphi_l(2) d\tau_2 \\ &= \sum_k \int \varphi_k^*(2) \frac{1 - P_{12}}{r_{12}} \varphi_k(2) d\tau_2 \end{aligned} \tag{5-10}$$

Consequently, we can write the SCF canonical equation as

$$\mathcal{F}(1)\varphi_v(1) = \epsilon_v \varphi_v(1) \tag{5-11}$$

However, thirdly, the canonical orbitals are not typically localized in a region of space, but rather spread over many atoms. This complicates the interpretation of molecular orbitals in terms of chemical bonds which are mostly localized.

One of the features of the canonical orbital energies is that they may be interpreted as approximate ionization potentials. This is Koopmans' theorem and it involves the same unrelaxed molecular orbitals for the n-1 system as in the n electron system. For instance, the energy of an n electron system is

$$E(n) = \sum_i^n \langle i|h|i\rangle + \frac{1}{2} \sum_{i,j}^n \langle ij||ij\rangle \tag{5-12}$$

Provided the orbitals are frozen, the energy is very similar for the n-1 system.

$$E(n-1) = \sum_{i}^{n-1} \langle i|h|i\rangle + \frac{1}{2}\sum_{i,j}^{n-1} \langle ij||ij\rangle \tag{5-13}$$

The ionization potential (IP) is the difference between the n-1 and n electron energies

$$IP = E(n) - E(n-1) = -h_n - \frac{1}{2}\left(\sum_{j}\langle nj||nj\rangle + \sum_{i}\langle in||in\rangle\right) = -\epsilon_n \tag{5-14}$$

which is also the orbital energy for whichever electron is removed.

5.2 $\bar{V}_{n-1}$ and $\bar{V}_{n-\alpha}$ Virtual Orbitals

With some inspection, it is easy to realize that the character of the occupied and virtual elements of the Fock matrix are quite different.

$$F_{pq} = h_{pq} + \sum_{i}^{n}\langle ip||iq\rangle \tag{5-15}$$

For the occupied orbitals, the effective potential terms cancel, so they are determined in the potential of n-1 electrons. However, for the virtual orbitals, p and q are never equal to i, so they are determined in the potential of n electrons, and hence, might be more appropriate for the n+1 electron system. Furthermore, since the HF energy is invariant to any definition of the virtuals, it might be beneficial to redefine them [147]. For CC or CI methods that include all excitations of single, double, etc. type, the computed energies and properties will be invariant to virtual orbital transformations. However, the invariance is lost if only a subset of the virtuals are retained. Thus, it is possible to define better virtuals where subsets retain most of the correlation energy, as they require much less time than the calculations in the full virtual space.

Kelly [148–152] investigated excluding different orbitals from v^{eff} to determine virtual orbitals and MBPT correlation energies for various orders. It is, however, somewhat ambiguous which occupied orbital should be excluded. A more

satisfactory route in modifying v^{eff} is to exclude each occupied orbital in an averaged way [153].

$$\bar{V}_{n-1} = \frac{n-1}{n} v^{eff} \tag{5–16}$$

It is also possible to envision excluding a larger number of electrons or even fractional numbers of electrons. There ultimate justification will be that a larger amount of correlation energy is obtained in a smaller subspace. If this is done in the same averaged way, the new potential has the form

$$\bar{V}_{n-\alpha} = \frac{n-\alpha}{n} v^{eff} \tag{5–17}$$

Numerical results for the $\bar{V}_{n-1}$ and $\bar{V}_{n-\alpha}$ potentials where α is the number of valence electrons are presented in Section 5.5.

5.3 Density Functional Theory Virtual Orbitals

Although originally formulated for solids, today, density functional theory (DFT) is routinely applied to atoms and molecules [154]. The one-particle Kohn-Sham equations are very similar in form to the Hartree-Fock equations, except that the Kohn-Sham effective potential is

$$v^{eff}(\mathbf{r}) = \frac{\partial J[\rho]}{\partial \rho(\mathbf{r})} + \frac{\partial E_{xc}[\rho]}{\partial \rho(\mathbf{r})} \tag{5–18}$$

In Kohn-Sham theory, v^{eff} contains Coulomb repulsion, exchange, and correlation, and in principle is exact provided the exchange-correlation functional is correct. One open question is how DFT virtual orbitals will perform in high-level CC calculations, since unlike SCF orbitals an electron in an occupied or virtual orbital feels the same potential. In Section 5.5, CC correlation energies using virtual orbitals from the LDA/VWN [155,156] and PW91 [157] functionals are presented and compared with other choices for the virtual space.

5.4 Frozen Natural Orbitals

Natural orbitals were introduced by Dirac [158] and extensively studied by Löwdin [159]. They are defined as the eigenvectors of the one-particle density matrix and provide the fastest convergence of the configuration-interaction (CI) expansion [159,160]. One of the potential problems with natural orbitals is that a correlated wave function is needed for their determination. (They can also be determined from orthogonalizing the Feynman-Dyson amplitudes using some self-energy approximation [161,162]). Several authors, including Meyer [163], used pseudo-natural orbitals obtained from an approximate density matrix at a lower level of theory to generate the natural orbitals. Since the density matrix is from a lower level of theory, the generation of pseudo-natural orbitals does not involve any rate limiting steps or is not a bottleneck for the calculation.

In practice, it is advantageous if there are no off-diagonal occupied-occupied, f_{ij}, or virtual-virtual, f_{ab}, elements in the Fock matrix, since these can force an iterative solution. For example with CCSD(T), the T_3 amplitudes are given by [164]

$$\begin{aligned} D^{abc}_{ijk} t^{abc}_{ijk} &= \sum_e P(i/jk)P(a/bc) t^{ae}_{jk} \langle bc||ei\rangle - \sum_m P(i/jk)P(a/bc) t^{bc}_{mi} \langle jk||ma\rangle \\ &\quad + P(i/jk)P(a/bc)\left[t^a_i \langle bc||jk\rangle + f_{ia} t^{bc}_{jk}\right] \\ &\quad - P(i/jk) \times \sum_m (1-\delta_{im}) f_{im} t^{abc}_{jkm} \times \sum_e (1-\delta_{ae}) f_{ae} t^{bce}_{ijk} \end{aligned} \tag{5-19}$$

The last terms in Equation 5–19 contain f_{im} and f_{ae} elements coupled to T_3. If the f_{im} or f_{ae} elements are not zero, the T_3 amplitudes appears on both sides of the equation and it must be solved iteratively. However, we can use the invariance of CC theory to orbital rotations among the occupied and virtual spaces to choose to make a semicanonical transformation of the resultant Fock matrix to simplify the solution of Equation 5–19. With semicanonical orbitals, the f_{ij} (i≠j) and f_{ab} (a≠b) elements are zero, however, the Fock matrix does contain f_{ia} terms. Since the f_{ia}

elements are coupled to T_2 amplitudes instead of T_3's in Equation 5–19, they do not force an iterative solution.

One close approximation to natural orbitals that avoids the complications of f_{ij} (i≠j), f_{ab} (a≠b), and even f_{ia} terms in energy calculations is frozen natural orbitals (FNOs) [165]. In this approach, only the virtual-virtual block of the one particle density matrix is diagonalized to generate natural orbitals constrained to the virtual space. Within the full virtual space, FNOs are just a unitary transformation of the original (e.g., Hartree-Fock) orbitals, so the energy is invariant. However, FNOs can achieve nearly all of the energy in a smaller space which provides considerable savings in the resulting calculation. Since some virtual orbitals are excluded from the resulting calculation or dropped, the energy is no longer invariant. Furthermore, the active block of the virtual-virtual Fock matrix can be diagonalized, so there are no f_{ab} (a≠b) terms which need to included in the energy calculation. However, the Fock matrix is not block diagonal with respect to the active and inactive portions, so there are f_{ab} (a≠b) terms within the inactive space which are pertinent in gradient calculations. Some numerical results of FNOs taken from a MBPT(2) wave function are shown in the next section.

5.5 Illustrative Examples

Table 5–1. Percent of total CCSD and CCSD(T) correlation energies recovered for different orbital choices. The molecular system is CO with r = 1.12832 Å [5].

	Percent of virtual space (number of virtual orbitals)					
	CCSD			CCSD(T)		
	80%(82)	60%(62)	40%(41)	80%	60%	40%
SCF	89.4	77.0	46.7	89.2	76.4	46.6
$\hat{V}_{n-1}$	90.0	78.9	53.6			
$\hat{V}_{n-\alpha}$	95.7	90.1	48.8			
LDA/VWN	89.4	77.1	46.8			
PW91	89.4	77.1	46.7			
FNO	100.0	99.4	97.1	100.0	99.4	96.9

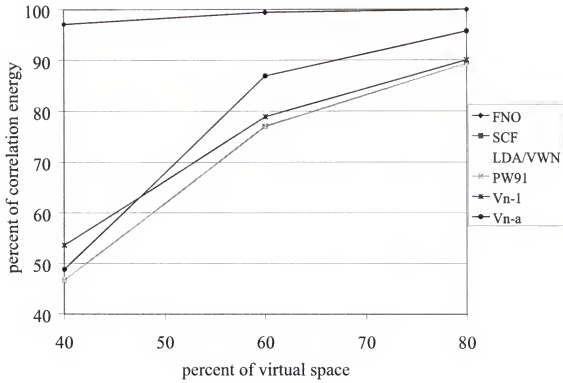

Figure 5–1. Percent of total CCSD correlation energies recovered for different orbital choices. The molecular system is CO.

In this section, a number of examples are considered to show the numerical performance of different orbital choices in a reduced space. In Table 5–1, the percentage of the correlation energy is tabulated for different choices of the orbital space and truncations of that space. The molecule is CO described in an aug-cc-pVTZ basis with all core electrons frozen. The results are also presented graphically in Figure 5–1. The SCF, LDA/VWN, and PW91 virtual orbitals recover nearly identical amounts of the CCSD correlation energy for the three truncations of the space. The $\bar{V}_{n-1}$ and $\bar{V}_{n-\alpha}$ results recover slightly more of correlation energy in the reduced spaces. However, the FNOs perform much better for both the CCSD and CCSD(T) correlation methods. For CCSD, FNOs achieve 100.0%, 99.4%, and 97.1% of the correlation energy in 80%, 60%, and 40% of the virtual space, respectively.

Table 5–2. Percent of total CCSD and CCSD(T) correlation energies recovered for different orbital choices. The molecular system is C_2H_4 with r_{CC} = 1.3342 Å, r_{CH} = 1.0812 Å, and a_{CCH} = 121.3 [5].

	Percent of virtual space (number of virtual orbitals)					
	CCSD			CCSD(T)		
	80%(162)	60%(121)	40%(81)	80%	60%	40%
SCF	95.6	78.5	55.6	95.5	77.8	54.6
$\bar{V}_{n-1}$	95.8	79.9	61.6			
$\bar{V}_{n-\alpha}$	97.3	90.1	48.6			
LDA/VWN	95.5	77.0	56.0			
PW91	95.5	76.9	56.0			
FNO	100.0	99.8	98.6	100.0	99.8	98.5

Table 5–3. Percent of total CCSD and CCSD(T) correlation energies recovered for different orbital choices. The molecular system is F_2 with r = 1.41193 Å [5].

	Percent of virtual space (number of virtual orbitals)					
	CCSD			CCSD(T)		
	80%(81)	60%(61)	40%(40)	80%	60%	40%
SCF	89.1	74.6	52.8	88.9	74.2	52.5
$\bar{V}_{n-1}$	89.6	76.1	52.8			
$\bar{V}_{n-\alpha}$	96.8	90.0	53.2			
LDA/VWN	89.1	74.6	52.8			
PW91	89.0	74.5	52.8			
FNO	99.8	98.7	93.2	99.8	98.6	92.8

Tables 5–2 through 5–5 present additional results for the C_2H_4, F_2, H_2O, and NH_3 molecular systems. One additional trend is that the $\bar{V}_{n-\alpha}$ potential performs better for 80% and 60% reductions of the virtual space, but the $\bar{V}_{n-1}$ potential performs slightly better for the 40% reduction of the virtual space.

Because total energies are seldom important, it is more constructive to examine computed energy differences. In Table 5–6, activation energies for the unimolecular dissociation of the pentazole anion, N_5^-, are presented. Again the SCF, LDA/VWN, and PW91 results are quite similar. The results for the FNOs are remarkably good. For the CCSD(T) method, FNOs with only 40% of the virtual space predict an

Table 5–4. Percent of total CCSD and CCSD(T) correlation energies recovered for different orbital choices. The molecular system is H_2O with r_{OH} = 0.9572 Å and a_{HOH} = 104.52 [5].

	Percent of virtual space (number of virtual orbitals)					
	CCSD			CCSD(T)		
	80%(80)	60%(60)	40%(40)	80%	60%	40%
SCF	85.5	73.8	38.0	85.2	73.2	38.1
$\tilde{V}_{n-1}$	87.0	77.1	48.0			
$\tilde{V}_{n-\alpha}$	95.8	90.6	4.7			
LDA/VWN	85.5	73.8	38.0			
PW91	85.5	73.7	38.2			
FNO	100.0	99.7	98.3	100.0	99.7	98.2

Table 5–5. Percent of total CCSD and CCSD(T) correlation energies recovered for different orbital choices. The molecular system is NH_3 with r_{NH} = 1.0116 Å and a_{NHN} = 106.7 [5].

	Percent of virtual space (number of virtual orbitals)					
	CCSD			CCSD(T)		
	80%(100)	60%(75)	40%(50)	80%	60%	40%
SCF	90.9	77.9	47.1	90.6	77.1	46.4
$\tilde{V}_{n-1}$	93.0	80.5	59.0			
$\tilde{V}_{n-\alpha}$	97.4	92.2	17.1			
LDA/VWN	90.9	77.8	47.2			
PW91	90.9	77.8	47.0			
FNO	100.0	99.8	98.7	100.0	99.8	98.6

activation energy of 29.3 kcal mol^{-1}. This is within 1 kcal mol^{-1} of the CCSD(T) result for the full virtual space, 28.8 kcal mol^{-1}.

Table 5–6. Activation energies in kcal mol^{-1} for different orbital choices. The percent of the total activation energy is shown in parentheses. The molecular system is N_5^- at the CCSD(T)/aug-cc-pVTZ ground and transition state optimized geometries.

	Percent of virtual space (number of virtual orbitals)							
	CCSD				CCSD(T)			
	100%(162)	80%(136)	60%(109)	40%(83)	100	80	60	40
SCF	34.7(100.0)	36.0(103.6)	32.5(93.6)	29.2(84.1)	28.8(100.0)	30.4(105.6)	27.0(93.8)	24.3(84.3)
$\bar{V}_{n-1}$		35.8(103.0)	32.2(92.7)	29.2(83.9)				
$\bar{V}_{n-\alpha}$		33.3(95.9)	29.4(84.6)	20.4(58.8)				
LDA/VWN		36.0(103.7)	32.6(93.7)	29.3(84.5)				
PW91		36.0(103.7)	32.6(93.8)	29.4(84.6)				
FNO		34.6(99.6)	35.2(101.3)	35.1(101.2)		28.7(99.6)	29.6(102.6)	29.3(101.6)

CHAPTER 6
CONCLUSIONS

Theoretical chemistry methods have a great potential to study, predict, and discover high-energy density materials. Often an initial theoretical survey can identify several promising highly energetic molecules that may be investigated further. In the more detailed work, theory can closely assist the experimental efforts. In fact CC methods have produced accurate structures and energetics, however, one of the bottlenecks in their conventional formulation and application is the dimension of the molecular orbital basis.

This dissertation has explored several different choices for the orbital space and the numerical results show that CC methods are largely invariant to different choices for the virtual orbital space including DFT, $\tilde{V}_{n-1}$, and $\tilde{V}_{n-\alpha}$ potentials. However, approximate frozen natural orbitals define a better virtual space of reduced dimension where much more of the correlation energy is recovered. The FNO procedure, detailed in Appendix A, constructs a reduced space with natural orbital information from the full space. Hence, FNOs achieve a large savings in the time needed per iteration of the CC equations. Although not investigated in this dissertation, FNOs might be useful in coupled-cluster equation-of-motion calculations for electronically excited, ionized and attached states. Additional future work could extend analytical gradient techniques for references with FNO reductions of the virtual space.

APPENDIX A
COMPUTATIONAL IMPLEMENTATION

The ability to generate frozen natural orbitals has been implemented into the ACES II suite of computer programs [68]. The following is a summary of the procedures performed by the xfno ACES member executable. It is important to note that in the limit of the full virtual space (i.e., δ=0), this procedure results in canonical Hartree-Fock virtual orbitals.

- The virtual-virtual block of the relaxed one-particle density matrix is calculated. For MBPT(2), this is:

$$D_{ab} = \frac{1}{2} \sum_{i,j,c} \frac{\langle ij||ac\rangle \langle ij||bc\rangle}{(\epsilon_i + \epsilon_j - \epsilon_a - \epsilon_c)(\epsilon_i + \epsilon_j - \epsilon_b - \epsilon_c)} \tag{A–1}$$

- Frozen natural orbitals, U, and their occupation numbers are obtained by diagonalizing this matrix:

$$U^{\dagger} D_{ab} U = u \tag{A–2}$$

- The natural orbitals are transformed to the basis of symmetry-adapted orbitals.

$$\underset{\text{so}}{\overset{\text{vrt}}{C}} \underset{\text{vrt}}{\overset{\text{vrt}}{U}} = \underset{\text{so}}{\overset{\text{vrt}}{U'}} \tag{A–3}$$

- The virtual-virtual block of the Fock matrix is built in the basis of natural orbitals.

$$\underset{\text{vrt}}{\overset{\text{so}}{U'^{\dagger}}} \underset{so}{\overset{\text{so}}{F}} \underset{\text{so}}{\overset{\text{vrt}}{U'}} = \underset{\text{vrt}}{\overset{\text{vrt}}{F'}} \tag{A–4}$$

- The active block of the Fock matrix is diagonalized to produce new orbital energies for the reduced space. The orbital energies for the reduced space are always larger than the original orbital energies.

$$\underset{\text{vrt}-\delta}{\overset{\text{vrt}-\delta}{Z^{\dagger}}} \underset{\text{vrt}-\delta}{\overset{\text{vrt}-\delta}{F'}} \underset{\text{vrt}-\delta}{\overset{\text{vrt}-\delta}{Z}} = \epsilon' \tag{A–5}$$

- The orbitals are updated to diagonalize the active virtual block of the Fock matrix.

$$\underset{\text{so}}{\overset{\text{vrt}-\delta}{U'}} \underset{\text{vrt}-\delta}{\overset{\text{vrt}-\delta}{Z}} = \underset{\text{so}}{\overset{\text{vrt}-\delta}{U''}} \tag{A–6}$$

REFERENCES

[1] Bartlett, R. J.; Stanton, J. F. Applications of Post-Hartree-Fock Methods: A Tutorial. In *Reviews in Computational Chemistry*; Lipkowitz, K. B.; Boyd, D. B., Eds.; VCH Publishers: New York, 1994.

[2] Bartlett, R. J. Coupled-Cluster Theory: An Overview of Recent Developments. In *Modern Electronic Structure Theory, Part I*; Yarkony, D. R., Ed.; World Scientific Publishing: Singapore, 1995.

[3] Lee, T. J.; Scuseria, G. E. Achieving Chemical Accuracy with Coupled-Cluster Theory. In *Quantum-Mechanical Electronic Structure Calculations with Chemical Accuracy*; Langhoff, S. R., Ed.; Kluwer: Boston, 1995.

[4] Taylor, P. R. Coupled-Cluster Methods in Quantum Chemistry. In *Lecture Notes in Quantum Chemistry II*; Roos, B. O., Ed.; Springer-Verlag: New York, 1994.

[5] Helgaker, T.; Jørgensen, P.; Olsen, J. *Modern Electronic Structure Theory;* John Wiley and Sons Ltd: West Sussex, 2000.

[6] Monkhorst, H. *Int. J. Quantum Chem. Symposium* **1977,** *11,* 421.

[7] Kucharski, S. A.; Kolaski, M.; Bartlett, R. J. *J. Chem. Phys.* **2001,** *114,* 692.

[8] Musial, M.; Kucharski, S. A.; Bartlett, R. J. *Chem. Phys. Lett.* **2000,** *320,* 542.

[9] Hirata, S.; Bartlett, R. J. *Chem. Phys. Lett.* **2000,** *321,* 216.

[10] Nooijen, M.; Bartlett, R. J. *J. Chem. Phys.* **1996,** *104,* 2652.

[11] Szalay, P. G.; Gauss, J. *J. Chem. Phys.* **1997,** *107,* 9028.

[12] Nooijen, M.; Lotrich, V. *J. Mol. Struct. (Theochem)* **2001,** *547,* 253.

[13] Olah, G. A.; Squire, D. R., Eds.; *Chemistry of Energetic Materials;* Harcourt Brace Jovanovich: San Diego, CA, 1991.

[14] Bartlett, R. J. *Chem. Ind.* **2000,** *4,* 140.

[15] Schmidt, M. W.; Gordon, M. S.; Boatz, J. A. *Int. J. Quantum Chem.* **2000,** *76,* 434.

[16] Guest, M. F.; Hillier, I. H.; Saunders, V. R. *J. Chem. Soc., Faraday Trans. 2* **1972,** *68*, 2070.

[17] Wright, J. S. *J. Am. Chem. Soc.* **1974,** *96*, 4753.

[18] Venanzi, T. J.; Schulman, J. M. *Mol. Phys.* **1975,** *30*, 281.

[19] Trinquier, G.; Malrieu, J.; Daudley, J. *Chem. Phys. Lett.* **1981,** *80*, 552.

[20] Novaro, O.; Castillo, S. *Int. J. Quantum Chem.* **1984,** *26*, 411.

[21] Lauderdale, W. J.; Myers, M. J.; Bernholdt, D. E.; Stanton, J. F.; Bartlett, R. J. The Search for Tetrahedral N_4. In *Proceedings of the High Energy Density Matter Contractors Conference at Long Beach, CA*; Air Force Office of Scientific Research: Building 410, Bolling AFB, Washington, DC 20332-6448, 1990.

[22] Francl, M. M.; Chesick, J. P. *J. Phys. Chem.* **1990,** *94*, 526.

[23] Lee, T. J.; Rice, J. E. *J. Chem. Phys.* **1991,** *94*, 1215. It should be noted that there is an error in the calculated zero-point energy effects on the $N_4 \longrightarrow 2N_2$ dissociation energies in this paper. The CCSD/ANO [4s3p2d1f] and CCSD(T)/ANO[4s3p2d1f] dissociation energies in Table 5 should read as follows: 193.3 and 182.9 kcal mol^{-1}, respectively.

[24] Lauderdale, W. J.; Stanton, J. F.; Bartlett, R. J. *J. Phys. Chem.* **1992,** *96*, 1173.

[25] Yarkony, D. R. *J. Am. Chem. Soc.* **1992,** *114*, 5406.

[26] Dunn, K. M.; Morokuma, K. *J. Chem. Phys.* **1995,** *102*, 4904.

[27] Korkin, A. A.; Balkova, A.; Bartlett, R. J.; Boyd, R. J.; von Ragué Schleyer, P. *J. Phys. Chem.* **1996,** *100*, 5702.

[28] Perera, S. A.; Bartlett, R. J. *Chem. Phys. Lett.* **1999,** *314*, 381.

[29] Bittererová, M.; Brinck, T.; Östmark, H. *J. Phys. Chem. A* **2000,** *104*, 11999.

[30] Bittererová, M.; Brinck, T.; Östmark, H. *Chem. Phys. Lett.* **2001,** *340*, 597.

[31] Zheng, J. P.; Waluk, J.; Spanget-Larsen, J.; Blake, D. M.; Radziszewski, J. G. *Chem. Phys. Lett.* **2000,** *328*, 227.

[32] Östmark, H.; Lanunila, O.; Wallin, S.; Tryman, R. *J. Raman Spectrosc.* **2001,** *32*, 195.

[33] Huisgen, R.; Ugi, I. *Ang. Chem. Int. Ed.* **1956,** *68*, 705.

[34] Ugi, I.; Perlinger, H.; Behringer, L. *Chem Ber.* **1958,** *91*, 2324.

[35] Ugi, I. . In *Comprehensive Heterocyclic Chemistry*; Katritzky, A. R.; Rees, C. W., Eds.; Pergamon Press: Oxford, 1984.

[36] Butler, R. N. . In *Comprehensive Heterocyclic Chemistry II*; Katritzky, A. R.; Rees, C. W.; Scriven, E. F. V., Eds.; Pergamon Press: Oxford, 1996.

[37] Christe, K. O.; Wilson, W. W.; Sheehy, J. A.; Boatz, J. A. *Angew. Chem. Int. Ed. Engl.* **1999,** *38*, 2004.

[38] Christe, K. O.; Dixon, D. A.; Mclemore, D.; Wilson, W. W.; Sheehy, J. A.; Boatz, J. A. *J. Fluor. Chem.* **2000,** *101*, 151.

[39] Vij, A.; Wilson, W. W.; Vij, V.; Tham, F. S.; Sheehy, J. A.; Christe, K. O. *J. Am. Chem. Soc.* **2001,** *123*, 6308.

[40] Fau, S.; Bartlett, R. J. *J. Phys. Chem. A* **2001,** *105*, 4096.

[41] Gagliardi, L.; Orlandi, G.; Evangelisti, S.; Roos, B. O. *J. Chem. Phys.* **2001,** *114*, 10733.

[42] Wang, H.; Law, C. K. *J. Phys. Chem. B* **1997,** *101*, 3400.

[43] Fau, S.; Wilson, K. J.; Bartlett, R. J. *J. Phys. Chem. A* **2002,** *106*, in press.

[44] Nguyen, M. T.; Sana, M.; Leroy, G.; Elguero, J. *Can. J. Chem.* **1983,** *61*, 1435.

[45] Nguyen, M. T.; McGinn, M. A.; Hegarty, A. F.; Elguero, J. *Polyhedron* **1985,** *4*, 1721.

[46] Chen, C. *Int. J. Quantum Chem.* **2000,** *80*, 27.

[47] Nguyen, M. T.; Ha, T. K. *Chem. Phys. Lett.* **2001,** *335*, 311.

[48] Ferris, K.; Bartlett, R. J. *J. Am. Chem. Soc.* **1992,** *114*, 8302.

[49] Burke, L. A.; Butler, R. N.; Stephens, J. C. *J. Chem. Soc., Perkin Trans. 2* **2001,** *9*, 1679.

[50] Gagliardi, L.; Pyykkö, P. *J. Am. Chem. Soc.* **2001,** *123*, 9700.

[51] Slater, J. C. *Phys. Rev.* **1928,** *31*, 333.

[52] Kato, T. *Commun. Pure Appl. Math.* **1957,** *10*, 151.

[53] Scuseria, G. E.; Ayala, P. Y. *J. Chem. Phys.* **1999,** *111*, 8330.

[54] Lewis, G. N. *J. Am. Chem. Soc.* **1924,** *46*, 2027.

[55] Dianov-Klonov, V. I. *Opt. Spect.* **1959,** *6*, 290.

[56] Leckenby, R. E.; Robins, E. J. *Proc. R. Soc. London A* **1965,** *265*, 389.

[57] Long, C. A.; Ewing, G. E. *J. Chem. Phys.* **1972,** *58*, 4824.

[58] Adamantides, V.; Neisius, D.; Verhaegen, G. *Chem. Phys.* **1980,** *48*, 215.

[59] Seidl, E. T.; Schaefer, III, H. F. *J. Chem. Phys.* **1988,** *88*, 7043.

[60] Dunn, K. M.; Scuseria, G. E.; Schaefer, III, H. F. *J. Chem. Phys.* **1990,** *92*, 6077.

[61] Seidl, E. T.; Schaefer, III, H. F. *J. Chem. Phys.* **1992,** *96*, 1176.

[62] Røeggen, I.; Nilssen, E. W. *Chem. Phys. Lett.* **1989,** *157*, 409.

[63] Hotokka, M.; Pyykkö, P. *Chem. Phys. Lett.* **1989,** *157*, 415.

[64] Bevsek, H. M.; Ahmed, M.; Peterka, D. S.; Sailes, F. C.; Suits, A. G. *Faraday Discuss.* **1997,** *108*, 131.

[65] Ahmed, M.; Blunt, D. A.; Chen, D.; Suits, A. G. *J. Chem. Phys.* **1997,** *106*, 7617.

[66] Eppink, A. T. J. B.; Parker, D. H. *Rev. Sci. Instr.* **1997,** *68*, 3477.

[67] Suits, A. G.; Houston, P. L. Alignment Effects and Imaging: Boon or Bane?. In *Workshop on Imaging Methods in Molecular Structure and Dynamics*; Neve Ilan, Israel, 1994.

[68] ACES II (Advanced Concepts for Electronic Structure) is a product of the Quantum Theory Project, University of Florida. Authors: J. F. Stanton, J. Gauss, J. D. Watts, M. Nooijen, N. Oliphant, S. A. Perera, P. G. Szalay, W. J. Lauderdale, S. Kucharski, S. R. Gwaltney, S. Beck, A. Balková, D. E. Bernholdt, K. K. Baeck, P. Rozyczko, J. Pittner, K. J. Wilson, H. Sekino, C. Huber, and R.J. Bartlett. Integral packages included are: VMOL (J. Almlöf and P. R. Taylor); VPROPS (P. R. Taylor); ABACUS (T. U. Helgaker, H. J. Aa. Jensen, P. Jørgensen, J. Olsen and P. R. Taylor).

[69] Basis sets were obtained from the Extensible Computational Chemistry Environment Basis Set Database, Version 1.0, as developed and distributed by the Molecular Science Computing Facility, Environmental and Molecular Sciences Laboratory which is part of the Pacific Northwest Laboratory, P.O. Box 999, Richland, Washington 99352, USA, and funded by the U.S. Department of Energy. The Pacific Northwest Laboratory is a multi-program laboratory operated by Battelle Memorial Institue for the U.S. Department of Energy under contract DE-AC06-76RLO 1830. Contact David Feller, Karen Schuchardt or Don Jones for further information.

[70] Lindh, R.; Barnes, L. A. *J. Chem. Phys.* **1994,** *100*, 224.

[71] Nooijen, M.; Bartlett, R. J. *J. Chem. Phys.* **1997,** *107*, 6812.

[72] Stanton, J. F.; Gauss, J. *Theor. Chim. Acta.* **1995,** *91,* 267.

[73] van der Zande, W. J.; Koot, W.; Los, J. *J. Chem. Phys.* **1989,** *91,* 4597.

[74] Saxon, R. P.; Liu, B. *J. Chem. Phys.* **1980,** *73,* 876.

[75] van der Zande, W. J.; Koot, W.; Los, J. *J. Chem. Phys.* **1988,** *89,* 6758.

[76] Helm, H.; Walter, C. W. *J. Chem. Phys.* **1993,** *98,* 5444.

[77] Dunn, K. M.; Morokuma, K. *J. Chem. Phys.* **1995,** *102,* 4904.

[78] Glukhovtsev, M. N.; Jiao, H.; von Ragué Schleyer, P. *Inorg. Chem.* **1996,** *35,* 7124.

[79] Gagliardi, L.; Evangelisti, S.; Widmark, P. O.; Roos, B. O. *J. Mol. Struct. (Theochem)* **1998,** *428,* 1.

[80] Tobita, M.; Wilson, K. J.; Fau, S.; Bartlett, R. J. *Structure and Stability of Polynitrogen Molecules and their Spectroscopic Characteristics.*, Quantum Theory Project, University of Florida, Gainesville, FL 32611-8435, http://www.qtp.ufl.edu/~bartlett.

[81] Wilson, K. J.; Beck, S. N.; Stanton, J. F.; Bartlett, R. J.; Miller, R. to be published.

[82] Korkin, A. A.; Bartlett, R. J. *J. Am. Chem. Soc.* **1996,** *118,* 12244.

[83] Friedman, A.; Soliva, A. M.; Nizkorodov, S. A.; Bieske, E. J.; Maier, J. P. *J. Phys. Chem.* **1994,** *98,* 8896.

[84] Hiraoka, K.; Nakajima, G. *J. Chem. Phys.* **1988,** *88,* 7709.

[85] Thompson, W. E.; Jacox, M. E. *J. Chem. Phys.* **1990,** *93,* 3856.

[86] Ruchti, T.; Speck, T.; Connelly, J. P.; Bieske, E. J.; Linnartz, H.; Maier, J. P. *J. Chem. Phys.* **1996,** *105,* 2591.

[87] Workentin, M. S.; Wagner, B. D.; Negri, F.; Zgierski, M. Z.; Lusztyk, J.; Siebrand, W.; Wayner, D. D. M. *J. Phys. Chem.* **1995,** *99,* 94.

[88] Workentin, M. S.; Wagner, B. D.; Lusztyk, J.; Wayner, D. D. M. *J. Am. Chem. Soc.* **1995,** *117,* 119.

[89] Tobita, M.; Bartlett, R. J. *J. Phys. Chem. A* **2001,** *105,* 4107.

[90] Rezchikova, K. I.; Churakov, A. M.; Burshtein, K. Y.; Shlyapochnikov, V. A.; Tartakovskii, V. A. *Mendeleev Comm.* **1997,** *5,* 174.

[91] Ovchinnikov, I. V.; Makhova, N. N.; Khmel'nitskii, I. I.; Kuz'min, V. S.; Akimova, L. N.; Pepekin, V. I. *Doklady Chemistry* **1998,** *359,* 67.

[92] Epishina, M. A.; Ovchinnikov, I. V.; Makhova, N. N. *Russ. Chem. Bull.* **1997,** *46,* 2117.

[93] Sheremetev, A. B.; Semenov, S. E.; Kuzmin, V. S.; Strelenko, Y. A.; Ioffe, S. L. *Chem. Eur. J.* **1998,** *4,* 1023.

[94] Q-Chem, Version 1.2, C. A. White, J. Kong, D. R. Maurice, T. R. Adams, J. Baker, M. Challacombe, E. Schwegler, J. P. Dombroski, C. Ochsenfeld, M. Oumi, T. R. Furlani, J. Florian, R. D. Adamson, N. Nair, A. M. Lee, N. Ishikawa, R. L. Graham, A. Warshel, B. G. Johnson, P. M. W. Gill and M. Head-Gordon, Q-Chem, Inc., Pittsburgh, PA, 1998.

[95] Dunning, Jr., T. H. *J. Chem. Phys.* **1989,** *90,* 1007.

[96] NBO 4.0. E. D. Glendening, J. K. Badenhoop, A. E. Reed, J. E. Carpenter, and F. Weinhold, Theoretical Chemistry Institute, University of Wisconsin, Madison, WI, 1996.

[97] Huber, K. P.; Herzberg, G. Constants of Diatomic Molecules. In *NIST Chemistry WebBook, NIST Standard Reference Database Number 69*; Mallard, W. G.; Linstrom, P. J., Eds.; National Institue of Standards and Technology: Gaithersburg, MD, 1998, http://webbook.nist.gov.

[98] Teffo, J. L.; Chendin, A. *J. Mol. Spectrosc.* **1989,** *135,* 389.

[99] Huheey, J. E.; Keiter, E. A.; Keiter, R. L. *Inorganic Chemistry Fourth Edition;* Harper Collins: New York, 1993, Appendix E.

[100] Galbraith, J. M.; Schaefer, III, H. F. *J. Am. Chem. Soc.* **1996,** *118,* 4860.

[101] Schulz, A.; Tornieporth-Oetting, I. C.; Klapöetke, T. M. *Angew. Chem Int. Ed. Engl.* **1993,** *32,* 1610.

[102] Klapöetke, T. M.; Schulz, A. *Chem. Ber.* **1995,** *128,* 201.

[103] Manaa, M. R.; Chabalowski, C. F. *J. Phys. Chem.* **1996,** *100,* 611.

[104] Doyle, M. P.; Maciejko, J. J.; Busman, S. C. *J. Am. Chem. Soc.* **1973,** *95,* 952.

[105] Klapöetke, T. M.; Schulz, A.; Tornieporth-Oetting, I. C. *Chem. Ber.* **1994,** *127,* 2181.

[106] Scuseria, G. E.; Schaefer, III, H. F. *J. Phys. Chem.* **1990,** *94,* 5552.

[107] Reed, A. E.; Weinstock, R. B.; Weinhold, F. *J. Chem. Phys.* **1985,** *83,* 735.

[108] Shaik, S. S.; Hiberty, P. C.; Ohanessian, G.; Lefour, J. M. *J. Phys. Chem.* **1988,** *92,* 5086.

[109] Glukhovtsev, M. N.; Simkin, B. Y.; Minkin, V. I. *Zh. Org. Khim.* **1988,** *24*, 2486.

[110] Glukhovtsev, M. N.; von Ragué Schleyer, P. *Chem. Phys. Lett.* **1992,** *198*, 547.

[111] Glukhovtsev, M. N.; von Ragué Schleyer, P. *Chem. Phys. Lett.* **1993,** *204*, 394.

[112] Gimarc, B. M.; Zhao, M. *Inorg. Chem.* **1996,** *35*, 3289.

[113] Gimarc, B. M.; Zhao, M. *Coord. Chem. Rev.* **1997,** *158*, 385.

[114] Afeefy, H. Y.; Liebmann, J. F.; Stein, S. E. Neutral Thermochemical Data. In *NIST Chemistry WebBook, NIST Standard Reference Database Number 69*; Mallard, W. G.; Linstrom, P. J., Eds.; National Institue of Standards and Technology: Gaithersburg, MD, 1998, http://webbook.nist.gov.

[115] Politzer, P.; Murray, J. S.; Grice, M. E.; Sjoberg, P. Computer-Aided Design of Monopropellants. In *Chemistry of Energetic Materials*; Olah, G. A.; Squire, D. R., Eds.; Harcourt Brace Jovanovich: San Diego, CA, 1991.

[116] Rosen, G. *Current Status of Free Radicals and Electronically Excited Metastable Species as High Energy Propellants;* NASA Technical Report: Pasadena, CA, 1973Report Number NASA-CR-136938, Contract Number NAS7-100 JPL-953623.

[117] Tobita, M.; Bartlett, R. J. *Predicted Structures and Spectroscopic Characteristics of Hydrazine, Lithium-Substituted Hydrazine and their Higher Derivatives.*, Quantum Theory Project, University of Florida, Gainesville, FL 32611-8435, http://www.qtp.ufl.edu/∼bartlett.

[118] Eaton, P. E.; Cole, Jr., T. W. *J. Am. Chem. Soc.* **1964,** *86*, 3157.

[119] Eaton, P. E. *Angew. Chem. Int. Ed. Engl.* **1992,** *31*, 1421.

[120] Eaton, P. E.; Gilardi, R. L.; Zhang, M. X. *Adv. Mater.* **2000,** *12*, 1143.

[121] Eaton, P. E.; Wicks, E. J. *J. Org. Chem.* **1988,** *53*, 5353.

[122] Eaton, P. E.; Xiong, Y.; Gilardi, R. *J. Am. Chem. Soc.* **1993,** *115*, 10195.

[123] Lukin, K. A.; Li, J.; Eaton, P. E.; Kanomata, N.; Hain, J.; Punzalan, E.; Gilardi, R. *J. Am. Chem. Soc.* **1997,** *119*, 9591.

[124] Zhang, M. X.; Eaton, P. E.; Gilardi, R. *Angew. Chem. Int. Ed.* **2000,** *39*, 401.

[125] Gilardi, R.; George, C.; Karle, J.; Eaton, P. E.; Fisher, A. M. *J. Heterocyclic Chem.* **1993,** *30*, 1385.

[126] Hehre, W. J.; Ditchfield, R.; Radom, L.; Pople, J. A. *J. Am. Chem. Soc.* **1970,** *92,* 4796.

[127] Hehre, W. J.; Radom, L.; von Ragué Schleyer, P.; Pople, J. A. *Ab Initio Molecular Orbital Theory;* Wiley-Interscience: New York, NY, 1986.

[128] Alkorta, I.; Elguero, J.; Rozas, I.; Balaban, A. T. *J. Mol. Struct. (Theochem)* **1990,** *206,* 67.

[129] Engelke, R. *J. Org. Chem.* **1992,** *57,* 4841.

[130] Engelke, R. *J. Am. Chem. Soc.* **1993,** *115,* 2961.

[131] Jursic, B. S. *J. Mol. Struct. (Theochem)* **2000,** *530,* 21.

[132] Gaussian 94, Revision C.3, M. J. Frisch, G. W. Trucks, H. B. Schlegel, P. M. W. Gill, B. G. Johnson, M. A. Robb, J. R. Cheeseman, T. Keith, G. A. Petersson, J. A. Montgomery, K. Raghavachari, M. A. Al-Laham, V. G. Zakrzewski, J. V. Ortiz, J. B. Foresman, J. Cioslowski, B. B. Stefanov, A. Nanayakkara, M. Challacombe, C. Y. Peng, P. Y. Ayala, W. Chen, M. W. Wong, J. L. Andres, E. S. Replogle, R. Gomperts, R. L. Martin, D. J. Fox, J. S. Binkley, D. J. Defrees, J. Baker, J. P. Stewart, M. Head-Gordon, C. Gonzalez, and J. A. Pople, Gaussian, Inc., Pittsburgh PA, 1995.

[133] Dunning, Jr., T. H. *J. Chem. Phys.* **1970,** *53,* 2823.

[134] Dunning, Jr., T. H.; Hay, P. J. Gaussian Basis Sets for Molecular Calculations. In *Methods of Electronic Structure Theory, Vol. 3*; Schaefer, III, H. F., Ed.; Plenum Press: New York, 1977.

[135] Redmon, L. T.; Purvis, G. D.; Bartlett, R. J. *J. Am. Chem. Soc.* **1979,** *101,* 2856.

[136] Dewar, M. J. S.; Zoebisch, E. G.; Healy, E. F.; Stewart, J. J. P. *J. Am. Chem. Soc.* **1985,** *107,* 3902.

[137] Bingham, R. C.; Dewar, M. J. S. *J. Am. Chem. Soc.* **1975,** *97,* 1294.

[138] Stewart, J. J. P. *J. Computat. Chem.* **1989,** *10,* 221.

[139] Raghavachari, K.; Trucks, G. W.; Pople, J. A.; Head-Gordon, M. *Chem. Phys. Lett.* **1989,** *157,* 479.

[140] Kybett, K. D.; Caroll, S.; Natalis, P.; Bonnell, D. W.; Margrave, J. L.; Franklin, J. L. *J. Am. Chem. Soc.* **1966,** *88,* 626.

[141] Kirklin, D. R.; Churney, K. L.; Donalski, E. S. *J. Chem. Thermodynamics* **1989,** *21,* 1105.

[142] Murray, J. S.; Seminario, J. M.; Lane, P.; Politzer, P. *J. Mol. Struct.* **1990,** *207*, 193.

[143] Cromer, D. T.; Ammon, H. L.; Holden, J. R. *A Procedure for Estimating the Crystal Densities of Organic Explosives;* Los Alamos National Laboratory: Los Alamos, NM, 1987LA-11142-MS.

[144] Taylor, C.; Cory, M.; Bartlett, R. J. to be published.

[145] Owens, F. J. *J. Mol. Struct.* **1999,** *460*, 137.

[146] Szabo, A.; Ostlund, N. S. *Modern Quantum Chemistry: Introduction to Advanced Electronic Structure Theory;* Dover Publications: Mineola, NY, 1996.

[147] Huzinaga, S.; Arnau, C. *Phys. Rev. A* **1970,** *1*, 1285.

[148] Kelly, H. P. *Phys. Rev.* **1963,** *131*, 684.

[149] Kelly, H. P. *Phys. Rev.* **1964,** *136*, B896.

[150] Kelly, H. P. *Phys. Rev.* **1966,** *144*, 39.

[151] Kelly, H. P. The Perturbation Theory of Brueckner and Goldstone Applied to Atoms. In *Perturbation Theory and its Application in Quantum Mechanics*; Wilcox, C. H., Ed.; Wiley: New York, 1966.

[152] Miller, J. H.; Kelly, H. P. *Phys. Rev. A* **1971,** *3*, 578.

[153] Silver, D. M.; Bartlett, R. J. *Phys. Rev. A* **1976,** *13*, 1.

[154] Parr, R. G.; Yang, W. *Density Functional Theory of Atoms and Molecules;* Oxford University Press: Oxford, 1989.

[155] Slater, J. C. *Quantum Theory of Molecules and Solids, Volume 4: The Self-Consistent Field for Molecules and Solids;* McGraw-Hill: New York, 1974.

[156] Vosko, S. H.; Wilk, L.; Nusair, M. *Can. J. Phys.* **1980,** *58*, 1200.

[157] Burke, K.; Perdew, J. P.; Wang, Y. Derivation of a Generalized Gradient Approximation: The PW91 Density Functional. In *Electronic Density Functional Theory: Recent Progress and New Directions*; Dobson, J. F.; Vignale, G.; Das, M. P., Eds.; Plenum Press: New York, 1997.

[158] Dirac, P. A. M. *P. Cambridge Phil. Soc.* **1930,** *26*, 376.

[159] Löwdin, P. O. *Phys. Rev.* **1955,** *97*, 1474.

[160] Hurley, A. C. *Electron Correlation in Small Molecules;* Academic Press: London, 1979.

[161] Reinhardt, W. P.; Doll, J. D. *B. Am. Phys. Soc.* **1968,** *13,* 1673.

[162] Reinhardt, W. P.; Doll, J. D. *J. Chem. Phys.* **1969,** *50,* 2767.

[163] Meyer, W. *J. Chem. Phys.* **1973,** *58,* 1017.

[164] Watts, J. D.; Gauss, J.; Bartlett, R. J. *J. Chem. Phys.* **1993,** *98,* 8718.

[165] Barr, T. L.; Davidson, E. R. *Phys. Rev. A* **1970,** *1,* 64.

BIOGRAPHICAL SKETCH

Kenneth John Wilson Jr. was born on September 13, 1975 in Youngstown, Ohio. The city of Youngstown in situated in northeastern Ohio, 120 miles south of Lake Erie, where much of the nation's steel was produced. Kenneth grew up in Youngstown, and attended public schools. He graduated fourth in a class of 195 from Woodrow Wilson High School on June 10, 1993. Then he studied at Youngstown State University, majored in chemistry, and graduated with a Bachelor of Science, Summa Cum Laude on June 21, 1997.

Kenneth enjoyed his time at the University of Florida and actively participated in many organizations. These include Mayors' Council (which advises UF's Division of Housing), Golden Key National Honor Society, Student Senate (which administers the Student Activity and Service Fee), The Honor Society of Phi Kappa Phi, and The International Honorary for Leaders in University Apartment Communities. Off campus, Kenneth served on the Bicycle and Pedestrian Advisory Committee (which advises the City of Gainesville, Alachua County, and the Metropolitan Transportation Planning Organization on transportation and long-range strategic-planning issues). During his service, he was involved with making the UF campus more bike- and pedestrian-friendly, and authored Student Senate Bill 2001-1069: Resolution to Improve Pedestrian Safety Along Village Drive. As one of twenty students during 2001, he was inducted into UF's Hall of Fame in recognition of outstanding service and achievement in the UF community. The Hall of Fame is located on the third floor of the Reitz Union and displays student portraits beginning from 1920.

I certify that I have read this study and that in my opinion it conforms to acceptable standards of scholarly presentation and is fully adequate, in scope and quality, as a dissertation for the degree of Doctor of Philosophy.

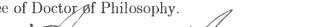

Rodney J. Bartlett, Chair
Graduate Research Professor of
Chemistry

I certify that I have read this study and that in my opinion it conforms to acceptable standards of scholarly presentation and is fully adequate, in scope and quality, as a dissertation for the degree of Doctor of Philosophy.

N. Yngve Öhrn
Professor of Chemistry

I certify that I have read this study and that in my opinion it conforms to acceptable standards of scholarly presentation and is fully adequate, in scope and quality, as a dissertation for the degree of Doctor of Philosophy.

Hendrik J. Monkhorst
Professor of Physics

I certify that I have read this study and that in my opinion it conforms to acceptable standards of scholarly presentation and is fully adequate, in scope and quality, as a dissertation for the degree of Doctor of Philosophy.

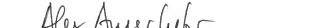

Alexander Angerhofer
Associate Professor of Chemistry

I certify that I have read this study and that in my opinion it conforms to acceptable standards of scholarly presentation and is fully adequate, in scope and quality, as a dissertation for the degree of Doctor of Philosophy.

Jeffrey L. Krause
Associate Professor of Chemistry

This dissertation was submitted to the Graduate Faculty of the Department of Chemistry in the College of Liberal Arts and Science and to the Graduate School and was accepted as partial fulfillment of the requirements for the degree of Doctor of Philosophy.

May 2002

_____

Dean, Graduate School